รายงานวิจัยฉบับสมบูรณ์

การเปลี่ยนรูป การผ่อนคลาย และการแตกตัวของอนุภาคในพอลิเมอร์ผสมแบบไม่เข้ากัน

รองศาสตราจารย์ ดร. อนุวัฒน์ ศิริวัฒน์

ตุลาคม 2549

สัญญาเลขที่ BRG 4680015

รายงานวิจัยฉบับสมบูรณ์

การเปลี่ยนรูป การผ่อนคลาย และการแตกตัวของอนุภาคใน พอลิเมอร์ผสมแบบไม่เข้ากัน

รองศาสตราจารย์ ดร. อนุวัฒน์ ศิริวัฒน์

วิทยาลัยปิโตรเลียมและปิโตรเคมี จุฬาลงกรณ์มหาวิทยาลัย

สนับสนุนโดยสำนักงานกองทุนสนับสนุนการวิจัย

ACKNOWLEDGEMENTS

The authors would like to acknowledge the funding provided by Thailand Research Fund through the Basic Research Grant no. BRG 4680015. Valuable suggestions and recommendations were kindly provided by Professor Ronald G. Larson from Department of Chemical Engineering, University of Michigan.

Table of Contents

Droplet Deformation Relaxation Breakup and Coalescence in Immiscible Polymer Blends
(Project Duration: 1 September 2003 – 31 August 2005)
(PI: Anuvat Sirivat)

Introduction

Problem Statements

Polymers that are recycled usually do not mix because of the unfavorable enthalpic interaction. During mixing of a major and a minor phases into a single blend, the blend is subject to usually complex shearing forces which result in the deformation, relaxation, breaking, and coalescence of the minor phase droplets. The resultant size distribution, and its various moments, control mechanical properties of the final solid state blend. Therefore, it is important to know key factors and/or conditions which influence the individual physical processes (deformation, relaxation, breakup, and coalescence) which lead to the final size distribution in the immiscible blend.

Droplet morphology of immiscible polymer blends depends on many factors: thermodynamic variables, rheological properties of individual polymers, and processing conditions. The understanding of the correlations between the blend morphology and the rheological properties in the past was based on Newtonian theories and are therefore inadequate to predict final blend physical/mechanical properties. The effects of viscoelastic properties, shearing conditions, interfacial tension, minor phase concentration on morphology of immiscible polymer blends subject to a simple *oscillatory* shear flow have not been previously addressed or understood. The *oscillatory* shear flow is a shear flow in which the applied stress or strain varies sinusoidally; it is a mode of shearing employed in many mixing devices.

Objectives

Our objective is to understand the relations between resultant blend morphology and its thermodynamic variables, rheological properties and processing conditions. If the proposed relations are available, then for a given polymer pairs in which we know the rheological properties and the processing conditions to be used, we can predict droplet size (mean value). The mean droplet size then can be used to predict several mechanical properties of the final solid state blend. Specifically, we will investigate the unexplored *oscillatory* flow mode on the deformation, relaxation, breakup, and coalescence processes.

Tasks Accomplished

We carried out various experiments to investigate the effect of unsteady shear flow on droplet deformation, relaxation, and breakup. In the first part (Chapters 1 and 2), we investigated the effects of frequency and amplitude of sinusoidal imposed shear strain on the droplet behaviors. We employed the polydimethyylsiloxan/polybutadiene material systems as the Newtonian blends and weakly elastic blends; both systems possess a small shear thinning behavior in the shear strain range studied.

Subsequently, we studied the same effect of frequency and amplitude on the droplet behavior of polyethylene/polystyrene material systems as the models of highly viscoelastic blends. In the second part (Chapters 3 and 4), we turned our attention to the transient droplet behaviors of highly viscoelastic blends of polyethylene/polystyrene material systems in which we observed for the first time the transient droplet deformation under steady stae shear flow. In the third part, we studied the effect of elasticity on the steady state droplet deformation in the steady state shear flow.

Outputs of TRF-BRG 4680015

Refereed Publications

1) Lerdwijitjarud, W., Sirivat, A., Larson, R.G. (2004) Influence of dispersed-phased elasticity on steady-state deformation and breakup of droplets in simple shearing flow of immiscible polymer blends. J. Rheology, v. 48(4), pp. 843-862.
(2004 ISI Impact Factor: 2.525)

2) Cherdhirankorn, T., Lerdwijitjarud, W., Sirivat, A., Larson, R. (2004) Dynamics of vorticity stretching and breakup of isolated viscoelastic droplets in an immiscible blends. Rheol. Acta. 43, pp. 246-256.
(2004 ISI Impact Factor: 1.558)

3) Tanpaiboonkul, T., Lerdwijitjarud, W., Sirivat, A., Larson, R. (2006)Transient and steady state deformations of dispersed –phase droplets of immiscible polymer blends in steady state shear flow. Submitted to Polymer.
(2004 ISI Impact Factor: 2.433)

4) Chanpaen, V., Lerdwijitjarud, W., Sirivat, A., (2006) Droplet deformation and breakup in Newtonian immiscible blends under oscillatory shear flow: effect of weak elasticity. Submitted to J. Rheology
(2004 ISI Impact Factor: 2.525)

5) Sirivat, A., Patako, S., Lerwijitjarud, W. (2006) Droplet deformation and breakup in viscoelatic immiscible blends under oscillatory shear flow. Submitted to Rheol. Acta.
(2004 ISI Impact Factor: 1.558)

Conference Proceedings

1) Lerdwijitjarud, W., Sirivat, A. Cheerdhirankorn, T. Solomon, M.J. (2003) Effect of dispersed phase elasticity on droplet deformation and breakup of immiscible polymer blends. 8th Pacific Polymer Conference, Bangkok, 24-27 November 2003.

Oral Presentations

1) Lerdwijitjarud, W., Sirivat, A., Larson, R. (2003) Non-Newtonian effect on morphology of immiscible polymer blends. RGJ-PhD Congress IV, Cholburi, 25-27 April 2003. *Selected as the best oral presentation in the Polymer Science and Engineering Session.*

2) Cherdhirankorn, T., Lerdwijitjarud, W., Sirivat, A., Larson, A. Dynamics of vorticity alignment and breakup of of viscoelastic droplets in an immiscible viscoelastic matrix under shear. AIChE Annual Meeting 2003, San Francisco, CA, 16-21 November 2003. (*Invited Talk Presented by Ronald Larson*)

3) Sirivat, A., Cherdhirankorn, T., Lerdwijitjarud, W., Larson, A. Droplet deformation relaxation and breakup in immiscible polymer blends. TRF "New Researchers Meet Senior Maethee Research Scholars", Petchaburi, 13-15 October 2005.
(*Invited spearker by A. Sirivat*).

Poster Presentations

1) Lerdwijitjarud, W., Larson, A., Sirivat, A. (2003)
Deformation and breakup of droplet in shearing flows of immiscible polymer blends: effect of constituent-component elasticity. Advances in Petrochemicals and Polymer in the New Millenium, Bangkok, 23-25 July 2003.

2) Sirivat, A., Cherdhirankorn, T., Lerdwijitjarud, W., Larson, R. (2003)
Transient deformation and breakup of isolated viscoelastic droplets in a viscoelastic matrix. AIChE Annual Meeting 2003, San Francisco, CA, 16-21 November 2003.

MS Graduates

1) Cherdhirankorn, T. (2003) Dynamics of Vorticity Stretching and Breakup of Isolated Viscoelastic Droplets in an Immiscible Viscoelastic Matrix. M.S. Thesis, Polymer Science, the Petroleum and Petrochemical College.

2) Tanpaiboobkul, P. (2004) Transient and Steady State Deformation of Dispersed-Phase Droplets in Immiscible Polymer blends in Steady State Shear Flow.
M.S. Thesis, Polymer Science, the Petroleum and Petrochemical College.

3) Janpaen, V. (2005) Oscillatory Shear Induced Droplet Deformation and Breakup in Immiscible Polymer Blends. MS thesis, Polymer Science, the Petroleum and Petrochemical College.

Chapter 1: Oscillatory Shear Induced Droplet Deformation And Breakup in Immiscible Polymer Blends

Vitsarut Janpaen [a], Wanchai Lerdwijitjarud [b], and Anuvat Sirivat [a *],

[a] Petroleum and Petrochemical College, Chulalongkorn University, Bangkok 10330, Thailand

[b] Department of Materials Science and Engineering, Faculty of Engineering and Industrial Technology, Silpakorn University, Nakhon Pathom 73000, Thailand

* Corresponding author: anuvat.s@chula.ac.th

Tel: 662 218 4131, Fax: 662 611 7221

OSCILLATORY SHEAR INDUCED DROPLET DEFORMATION AND BREAKUP IN IMMISCIBLE POLYMER BLENDS

Synopsis

Deformation and breakup of droplets in polybutadiene/polydimethylsiloxane blends subject to oscillatory shear flow were investigated experimentally using an optical shear flow cell. The apparent major axis (a*), the minor axis (c) in the vorticity direction of the droplets were measured as functions of time. From the time series of the deformation parameters, (a* - c)/(a* + c), we can define the deformation amplitudes as one halves the differences between the maximum and minimum values. The deformation parameters generally decreased with increasing viscosity ratio, time scale ratio and droplet elasticity. The dependence of the deformation parameters on capillary number is generally linear up to a certain value for Newtonian droplets, regardless of viscosity ratio and time scale ratio. The dependence becomes totally nonlinear with increasing droplet elasticity. Droplet viscosity and elasticity generally impede breakup under oscillatory shear. Critical capillary number for breakup, the number of resultant daughter droplets, and the number of cycle required for breakup to occur increase with time scale ratio. The apparent breakup pattern changes from the dumbbell type to the end-pinching type as time scale ratio increases.

I. INTRODUCTION

Droplet size, shape and their distributions as obtained from blending immiscible polymers are important factors which influence physical and mechanical properties of the blends. The resultant morphology is controlled by the physical, chemical, and rheological properties of individual polymers, as well as the processing conditions. The deformation and breakup of a suspended immiscible Newtonian droplet in another Newtonian matrix in a steady state shear flow was first investigated and studied by Taylor (1932, 1934). He suggested that the droplet deformation is controlled by two dimensionless numbers: the viscosity ratio, η_r which is the ratio between viscosity of droplet (dispersed phase) (η_d) and viscosity of matrix (η_m), and the Capillary number (Ca) or Taylor number, defined by the viscous force to the interfacial surface force:

$$Ca = \frac{\dot{\gamma}\,\eta_m D_0}{2\Gamma} \qquad (1)$$

where $\dot{\gamma}$ is the shear rate, D_o is initial droplet diameter and Γ is interfacial tension. For small deformations, the shape of droplet is ellipsoidal and its deformation is described by the parameter Def, given by:

$$\mathrm{Def} \equiv \frac{a-b}{a+b} = \mathrm{Ca}\,\frac{19\eta_r + 16}{16\eta_r + 16} \tag{2}$$

where a and b are the lengths of the major and minor axes of the deformed droplet (ellipsoidal shape), respectively. Taylor predicted that the critical point at which the viscous force overcomes the interfacial force leading to droplet breakup occurs at Ca_c (critical capillary number for droplet breakup) ≈ 0.5 and Def_c (critical deformation) ≈ 0.5 for a steady simple shearing flow (or quasi-steady), if the flow rate is very slowly increased with a viscosity ratio of around unity. These basic predictions have been later confirmed by several experiments [Rumscheid and Mason (1961); Grace (1982); Bentley and Leal (1986); Guido and Villone (1998)]. These results show that for Newtonian fluids, droplet deformation and breakup are strongly influenced by viscosity ratio. In simple shearing flow, no breakup occurs when the viscosity ratio is higher than four [Grace (1982)]. For steady state shearing of an isolated Newtonian droplet in a Newtonian matrix, the critical capillary number at which breakup occurs is minimized when the viscosity ratio is around unity [Grace (1982)].

In typical polymer blends, the viscoelasticity and the shear-thinning effect of individual components are expected to affect the droplet deformation and breakup. Droplet deformation and breakup in immiscible blend systems when either one or both phase is viscoelastic fluid have been studied by several workers [Flumerfelt (1972); Elmendrop and Maalcke (1985); Wu (1987); Milliken and Leal (1991); Varanasri *et al.* (1994); Levitt *et al.* (1996); Mighri *et al.* (1997, 1998); Hobbie and Migler (1999); Migler (2000); Mighri and Huneault (2001); Tretheway and Leal (2001); Lerdwijitjarud

et al. (2003, 2004); Cherdhirankorn *et al.* (2004)]. There is a thorough review of the literature on the influence of elasticity on droplet deformation and breakup reported in the earlier works [Cherdhirankorn *et al.* (2004)]. The main finding is that droplet elasticity suppresses droplet deformation and breakup, and can cause droplet widening, possibly due to the existing normal stresses.

Nearly all experimental work on droplet deformation and breakup reported in the literature has been carried out on droplets in steady simple shearing flow. The deformation and breakup of droplets in oscillatory shear are rare. Wannaborworn and Mackley (2002) was the first pioneering work to observe and investigate the deformation and breakup of immiscible Newtonian drops with a viscosity ratio of unity under oscillatory shear. For moderate strains, the drop deformation parameters varied sinusoidally between the maximum and the non-zero minimum values. At large strains, the drops breakup occurred through the pattern of end-pinching.

In the present work, we carried out further a systematic investigation of the droplet deformation and breakup in oscillatory shear flows. The immiscible polymer blends used were Newtonian fluids and the Boger fluids without shear thinning. In particular, we are interested in the influence of the viscosity ratio; it may be expected that a lower viscosity ratio value would favor larger droplet deformation and subsequent breakup, whereas a very large value would lead to a droplet solid body translation. The influence of time scale ratio, the droplet relaxation in the blend over the imposed oscillatory time scale, should also be important factor to investigate. In the limit of small time scale ratio, the droplet is expected to be deformed in a quasi-equilibrium

state; on the other hand, the limit of large time scale ratio would lead to a droplet solid body translation, irrespective of viscosity ratio. Lastly, the effect of droplet elasticity is expected to suppress droplet deformation and breakup, for given viscosity and time scale ratios. One of our objectives is to observe droplet deformation versus Capillary number in both linear and nonlinear regimes under the influences of the three factors mentioned. Another objective is to observe various possible breakup patterns, and the factors that control the number of resultant daughter droplets. The last finding may serve as relevant and useful knowledge for the emulsion or immiscible polymer processing.

II. EXPERIMENTS

A. Materials

The materials used in this study were polydimethylsiloxanes, PDMS, with viscosity value of 30,000 centiStoke (Viscasil 30M) (donated by General Electric International Operations Company, Inc.) as the matrix phases and a polybutadiene, PBd, (Ricon 150, donated by Chemical Innovation) as the dispersed phase. The properties of the blend components are listed in Table I. High-molecular-weight polybutadiene (M_w ~841,000 , M_w/M_n ~1.20 purchased from Fluka Chemical Corp.) was used as the high molecular weight polymer component additive for the Ricon 150 to make a "Boger" fluid [Boger and Binnington (1977)] with significantly higher elasticity but a slight shear thinning behavior. The polymer blend systems investigated are listed in Tables II, III, and IV.

B. Sample Preparation

PDMS's were used as received. Because of possible volatile components in PBd as received, it was vacuum dried at 50 °C until the volatile components were driven off and the weight loss discontinued. The elastic dispersed phases (for the blend systems B1 and B2 in Table IV) were prepared by completely dissolving a high molecular weight PBd into chloromethane. The solutions were mixed with small amounts of low molecular weight PBd at room temperature to obtain "Boger" fluids. The mixtures were left for five days to obtain homogenous solutions. The chloromethane and other volatile components were subsequently removed by vacuum drying at 50 °C.

C. Rheological Characterization

The storage modulus (G') and loss modulus (G") of each blend component were measured by a cone and plate rheometer (Rheometrics Scientific, model ARES), with 25-mm plate diameter with cone angle of 0.04 rad. and a gap of 0.051 mm. Because of the difference in temperature dependences of the viscosities of PBd and PDMS, a proper choice of operating temperature permits a blend of equal viscosity value, or a desired viscosity ratio between the two components (or equivalently a desired ratio between the values of G'' at the frequency of interest). From the rheological properties of pure polymers at various temperatures, the desired pairs of polymers and operating temperatures were selected for further study. The rheological properties are

shown in Figures 1, 2, and 3. In our study, we chose blend systems A1, A2, and A3 at G" ratios equal to 0.16, 1 and 3 at temperatures of 67, 33 and 20 °C, respectively. Since G" >> G' at all frequencies and temperatures investigated, both components of the blend systems A1-A3 can be considered to be pure viscous fluids with nearly zero elasticity.

D. Observation of an Isolated Droplet in an Oscillatory Shearing Flow

1. Shearing Apparatus

To observe the droplets in an oscillatory shear flow, we used a flow cell (Linkam CSS 450, Linkam Scientific Instruments Ltd.) consisting of two transparent quartz parallel disks mounted on an optical microscope (Leica DMRPX, Leica Imaging Systems LTd.), and connected to a CCD camera (Cohu 4910, Cohu Inc.). The observation window is located at 68 mm from the center. The images taken were analyzed on a computer using the Scion image software (www.scioncorp.com). To obtain isolated droplets, the PDMS matrix phase was first loaded into the flow cell. The PBd dispersed phase was added at low concentrations, i.e less than 1% in order to form

isolated droplets, into the matrix phase by using a microsyringe. To avoid wall-induced migration effects, only droplets near the center of the gap were chosen.

2. Droplet Shape Relaxation Time

The samples were loaded into the flow cell, and the temperature was adjusted to obtain a preselected G" ratio. We selected a droplet with an initial diameter of 200 (± 10%) μm. We imposed step strains on the sample with magnitude 0.5-20% and shear rates of 1, 2 and 3 rad/s. The deformation of the isolated droplet after a step strain was recorded.

Using the optical microscope, the droplet images were captured only from the top view; the true lengths of the principle axes cannot be directly measured as the droplet was tipped in a direction normal to the viewing plane. However, the lengths of these axes can be determined by assuming an affine angle of rotation of the droplet in plane containing the flow and shear-gradient directions together with the condition of volume preservation, $D_o^3 = abc$ (Almusallam *et al.* (2000)). Although the lengths of the principle axes can be appropriated by using the method mentioned above, we adopt to use the apparent lengths of the observable axes (i.e., projected into the observation plane) to describe the behavior of each droplet. We thus define a modified deformation parameter Def* as:

$$Def^* \equiv \frac{a^* - c}{a^* + c} \tag{3}$$

where a* and c are major and minor axis of droplet images obtained from the top view.

A time series of the retracting droplet deformation parameter Def* vs. time was computed, which has been found to decay exponentially as [Lucinia *et al.* (1997)]:

$$\mathrm{Def} = \mathrm{Def}_o \exp\left(-\frac{t}{\tau}\right) \tag{4}$$

The characteristic relaxation time for a single isolated droplet (τ) can be derived from a semi-logarithmic plot of droplet deformation parameter versus relaxation time. The slope of the straight line was fitted to the data in the linear relaxation regime [Luciani *et al.* (1997), Mo *et al.* (2000), Xing *et al.* (2000)]. By equating this characteristic relaxation time to that predicted by the Palierne model (Eq.3) [Palierne (1990) and Graebling *et al.* (1993)], the interfacial tension was then calculated from the following relation:

$$\tau = \frac{(3+2\eta_r)(16+19\eta_r)r_o\eta_{m,o}}{40(1+\eta_r)\Gamma} \tag{5}$$

where $\eta_r=\eta_d/\eta_m$ is the ratio between the dispersed phase viscosity and the matrix phase viscosity, Γ is the interfacial tension and r_o is the radius of the spherical drop. Two hundred to three hundred images were typically recorded (ten to twenty frames per second) while the droplet relaxed from the deformed shape to its original spherical shape.

3. Oscillatory Deformation

As before, a sample was loaded and the operating temperature and the size of the droplet were chosen. The shearing mode was sinusoidal oscillatory. The Linkham device, which has one stationary and one moving plate, typically causes the droplet to move back and forth. Before we started each experiment, the drop was allowed for relax until it retained a spherical shape. Appropriate strain and frequency were then chosen and applied.

We define the characteristic time scale ratio (τ_r) as the characteristic relaxation time scale (τ_{rel}) divided by the oscillatory time (τ_{osc} = 1/f, with f in Hertz), and we use it to describe the ability of droplet to relax its shape under an oscillatory shear flow at various frequencies. For the system A2, with a viscosity ratio equal to one, we considered τ_r values of 0.15, 0.45, and 0.79, corresponding to oscillating frequencies of f = 0.1, 0.3, and 0.52 Hz, respectively. For a given frequency, we increased the strain amplitude until we could no longer capture all images during a droplet deformation cycle. In each experiment, 600-700 images were recorded; for each period of deformation the number of captured images was equal to or greater than 32 in order to track the deformation time series in detail.

III. RESULTS AND DISCUSSION

A. Rheological Characterization

Figures 1 and 2 show the storage modulus (G') and the loss modulus (G") of blend components, respectively. The data indicate that the rheological responses of the

two polymers are in the terminal zone over the frequency range studied (up to 100 s^{-1}) since the slope of G' is approximately equal to two and the slope of G" is approximately equal to one on the log-log plots. Polydimethylsiloxane has a lower temperature-dependent viscosity than does polybutadiene, allowing us to obtain the desired ratios of G' or G" values for one component relative to the other by adjusting the operating temperature. Alternatively, we can vary the G' and G" ratios by using different molecular weights without changing the temperature. However, this later method is more time consuming and it is difficult to obtain the desired ratios and thus it was not employed in our work. The values of the G' and G" ratios used are shown in Figure 3.

In most of our experiments, the working fluids were highly viscous so G" ratio is more relevant than the G' ratio. In the experiment on the effect of viscosity ratio, G" ratio was equal to 0.16, 1 and 3 at 67°C, 33°C and 20°C (Table II). For the 0.02% high Mw PBd sol^{n} and the 0.05% high Mw PBd sol^{n}, G" ratio was equal to 1 at 27 °C and 25°C respectively, at all frequencies examined (Table IV).

B. Relaxation Experiment

The relaxation time scale of each blend studied was obtained from a step strain experiment. The values of interfacial tension values obtained were 3.85×10^{-3} N/m, 3.90×10^{-3} N/m, and 3.94×10^{-3} N/m, with the characteristic relaxation times equal to 0.5 sec., 1.5 sec. and 3.6 sec. for G''_r ratio equal to 0.16, 1 and 3, corresponding to temperatures of 67 °C, 33 °C, and 20 °C, respectively. For the 0.02% high Mw PBd sol^{n} and the 0.05% high Mw PBd sol^{n}, the interfacial tension values were equal to 3.94×10^{-3}

N/m and 4.09×10^{-3} N/m with the characteristic relaxation times equal to 1.8 and 1.7 sec, respectively.

C. Oscillatory Shear Experiment

In oscillatory shear, there are several parameters that can be grouped into dimensionless groups; namely the Capillary Number (Ca_m), Reynolds number (Re_{osc}). the time scale ratio (τ_r), and the Weissenberg number. Ca_m and Re are defined as:

$$Ca_m = \frac{G_m''(\omega)\gamma d}{\Gamma} \tag{6}$$

$$\mathrm{Re}_{osc} = \frac{\rho_d \omega^2 d^2}{G_d''(\omega)} \tag{7}$$

where γ is the strain amplitude imposed on the blends, d is the diameter of the droplet, $G_m''(\omega)$ is the loss modulus of the matrix phase, $G_d''(\omega)$ is the loss modulus of the dispersed phase, ρ_d is the density of the dispersed phase, and Γ is the interfacial tension between two polymers. In all experiments here, the Reynolds number is very small, less than 10^{-5}, and so inertial force is negligible. The time scale ratio is defined as:

$$\tau_r = \tau_{rel}/\tau_{osc} \tag{8}$$

where τ_{rel} is the relaxation time obtained from the relaxation experiment, τ_{osc} is the period of oscillation, $\tau_{osc} = 1/f$, where f is the oscillation frequency used.

The Weissenberg number, which is a dimensionless number used in the study in viscoelastic flows, is defined here as the ratio between the dispersed phase elasticity and the matrix phase shear stress at a particular shear rate:

$$Wi_d = 2G'_d(\omega)/G''_m(\omega)\gamma \qquad (9)$$

The values of the Weissenberg number of our blend systems investigated are shown in Tables II, III, and IV: system A1 (G''_r = 0.16, τ_r = 0.17), Wi_d = 0.0006-0.006; system A2 (G''_r = 1, τ_r = 0.15), Wi_d = 0.0034-0.034; system A2 (G''_r = 1, τ_r = 0.45), Wi_d = 0.0045-0.045; system A2 (G''_r = 1, τ_r = 0.79), Wi_d = 0.0057-0.057; system A3 (G''_r = 3.0, τ_r = 0.14), Wi_d = 0.0092-0.092; system B1 (0.02%high M_w PBd sol$^n_\perp$, G''_r = 1, τ_r = 0.18), Wi_d = 0.006-0.068; and system B2 (0.05%high M_w PBd sol$^n_\perp$, G''_r = 1, τ_r = 0.15), Wi_d = 0.018-0.186.

We divide our experimental work into 3 parts: the effects of the viscosity ratio, of Deborah number (or time scale ratio), and of elasticity ratio.

Figure 4 shows optical micrographs of a droplet under oscillatory deformation: G''_r = 1, Ca_m = 0.6, Re_{osc} = 2 x 10^{-8}, and τ_r = 0.15. The drop size was 200 μm. The droplet can be seen to stretch along the flow direction, to retract to its original value, to stretch again, and finally to retract back when the cycle is complete. We may note that droplet deformation in an oscillatory shear is distinct from that in steady shear due to the combination of the cyclic droplet rotation and the periodic changes in shear direction and amplitude.

Figure 5 shows the deformation amplitudes, a*, c, and Def* vs time for the droplet of Figure 4. We can see clearly that there is a period of an initial transient deformation, lasting about 8 seconds, prior to attainment of the final steady state oscillatory deformation. In the final steady state, we can define the deformation

amplitudes δa^*, δc, and δDef^* as one half of the differences between the maximum and the minimum values of the corresponding deformation parameters: a^*, c, and Def^*, respectively.

Figures 6a, 6b, and 6c show the steady state deformation amplitudes δa^*, δc, and δDef^* vs. Ca_m of the three blend systems A1, A2, and A3: G''_r = 0.16, 1.0 and 3.0. In these experiments, the oscillatory frequencies were chosen to be 0.35 Hz, 0.1 Hz, and 0.04 Hz, respectively, so that the corresponding time scale ratios are nearly the same value, i.e. 0.14 - 0.17. Ca_m was varied by varying strain amplitude up to the value in which all images in a cycle can be taken. Droplet sizes were ~ 200 μm. We can see that, for a given Ca_m, Def^* is greater for a droplet with a smaller G" ratio (or viscosity ratio). This implies that droplet viscosity resists droplet oscillatory deformation, a similar finding to that of the steady state shear flow. In Figure 6c, we may note that the relation between Def^* and Ca_m is linear when the G" ratio (or viscosity ratio) is 0.16 or 1.0. This may stem from the fact that for these two blends variations in Ca_m were small, below 1.2. On the other hand, for the blend of G" ratio equal to 3.0, the relation between Def^* and Ca_m is nonlinear. We also note that the deformation frequency, f_{def}, the inverse of the period of δa^*, δc, or δDef^* of these blends, are nearly the same as the excitation frequency, f_{osc}, for the ranges of Ca_m examined. The departure from linearity occurs through the amplitudes first.

Figure 7a, 7b and 7c show the deformation amplitudes δa^*, δc, and δDef^* vs. Ca_m of the blend system A2 at various time scale ratios: τ_r = 0.15, 0.45, and 0.79. The corresponding G''_r was fixed and equal to one. We can see that, for a given Ca_m, Def^* is

greater for a droplet with a smaller time scale ratio τ_r. A smaller time scale ratio means that droplet relaxes very fast relative to the deformation time scale so the droplet tends to be close to its equilibrium shape of a particular shear strain rate at any instants of time. On the other hand, when the time scale ratio is much greater than unity, the droplet cannot adjust its shape fast enough to attain the equilibrium shapes. In the limit of τ_r approaches infinity, we would expect Def* to attain its asymptotically low value in which Def* becomes independent of Ca_m and a 'frustrated' deformation state is attained.

Figures 8a, 8b and 8c show the amplitudes of the deformation parameters δa^*, δc, and δDef^* vs. Ca_m of three systems (Table IV): no elasticity, system A2; 0.02% high M_w PBd sol^n, system B1; and 0.05% high M_w PBd sol^n, system B2. G''_r were fixed at 1.0, and the variation in time scale ratios was relatively small, i.e. 0.15 – 0.18. The corresponding oscillatory frequencies were then 0.1 Hz for the zero-elasticity system, 0.099 Hz for the 0.02% high M_w PBd sol^n, and 0.087 Hz for the 0.05% high M_w PBd sol^n. We can observe from these figures that at small values of Ca_m, below 0.4, the amplitudes of the deformation parameters of the three systems are nearly the same. At $Ca_m > 0.4$, the non-elastic droplet deforms more than do the more elastic droplets at the same Ca_m. This implies that droplet elasticity resists droplet deformation.

Figures 9 and 10 show photographs of droplet breakup under oscillatory shear for system A1 (Table II, G'' = 0.16) at oscillatory frequencies of 0.05 Hz and 0.3 Hz, and the corresponding time scale ratios of 0.019 and 0.114, respectively for the chosen droplet size of ~150 μm. In Figure 9, at an oscillatory frequency equal to 0.05 Hz and time scale ratio of 0.019, the drop was observed to stretch along the flow direction. As

the amplitude of oscillation was increased further, the drop progressively deformed further and at the critical condition, the usual dumbbell shape leading to breakup was observed. The drop broke into two nearly equal parts, as shown in Fig. 9. This is a droplet breakup pattern presumably under its quasi-equilibrium state. In Figure 10, for a droplet of system A1 (Table I, G'' = 0.16) with oscillatory frequency of 0.30 Hz and time scale ratio of 0.114, the breakup pattern now assumes the end-pinching type. The obvious quantitative difference is that now there are four daughter droplets resulting from the breakup. The number of daughter droplets appears to increase with the time scale ratio. We also note that the numbers of cycle required for breakup to occur are approximately 1 and 48 for droplets of system A1 with time scale ratios of 0.019 and 0.114, respectively. Our results should be compared with those of Wannaborworn *et al.* [2000] in which they observed droplet breakup pattern to be end-pinching type along with many daughter drops for their system with G'' equal to one. Our experimental data of droplet breakup of system A2 (G'_r equal to one) also confirm their findings; we found end-pinching patterns, and in addition, along with more daughter droplets as time scale ratio increases.

Figure 11 shows the critical capillary number vs. time scale ratio for system A1, with $G''_r = 0.16$. The droplet size was ~ 150 μm. We can see that the critical Ca_m increases linearly with the time scale ratio; its intercept value at zero time scale ratio is approximately one. Finally, we may note that we were unable to observe drop breakup for system B2 with our present apparatus and experimental conditions allowed.

IV. CONCLUSIONS

From experimental measurements of droplet deformation in oscillatory shear, we have investigated the effects of viscosity ratio, time scale ratio, and elasticity on the Newtonian and Boger droplet deformation and breakup. The oscillatory amplitudes decrease with viscosity ratio, time scale ratio and the droplet elasticity. Droplet viscosity and elasticity impede oscillatory deformation. At low time scale ratio, droplet deformation varies with time under quasi-equilibrium state; for large time scale ratio, the visually apparent deformation can be referred to be in a frustrated state. The number of resultant daughter drops and the number of cycle required for breakup to occur increase with time scale ratio. The critical Ca_m increases linearly with time scale ratio. The breakup pattern changes from the dumbbell type to end-pinching with increasing time scale ratio.

ACKNOWLEDGEMENTS

The authors would like to thank General Electric International Operations Company Inc. for supplying polydimethylsiloxane (viscasil 30M), Chemical Innovation for supplying low molecular weight polybutadiene (Ricon 150). AS would like to acknowledge the funding from TRF, grant no. BRG4680015, and the funding from Conductive and Electroactive Research Unit, Chulalongkorn University. WL would like to thank Faculty of Engineering and Industrial Technology, Silpakorn University for partly supporting the research utility. We also would like to thank Professor Ronald G. Larson for his kind helps in preparing this manuscript.

REFERENCES

1. Almusallam A. S., R. G. Larson, and M. J. Solomon, "A constitutive model for the prediction of ellipsoidal droplet shapes and stresses in immiscibie blends", *J. Rheol* **44**, 1055-1083 (2000).
2. Bentley, B.J., and L. G. Leal, "An experimental investigation of drop deformation and breakup in steady, two-dimensional linear flows," *J. Fluid Mech.*, **167**, 241-283 (1986).
3. Boger, D. V. and R. J. Binnington, "Separation of elastic and shear thinning effects in the capillary rheometer", *Trans. Soc. Rheol.* **21**, 515-534 (1977).
4. Cherdhirankorn T., W. Lerdwijitjarud, A. Sirivat, and R. G. Larson, "Dynamics of Vorticity Stretching and Breakup of Isolated Viscoelastic Droplets in an Immiscible Viscoelastic Matrix" *Rheologica Acta* **43**, 246-256 (2004).
5. Elmendorp, J. J. and R. J. Maalcke, "A study on polymer blending microrheology: Part 1", *Polym Eng. Sci.* **25**, 1041-1047 (1985).
6. Flumerfelt, R. W."Drop breakup in simple shear fields of viscoelastic fluids", *Ind. Eng. Chem. Fundam.*, **11**, 312-318 (1972).
7. Grace, H. P., "Dispersion phenomena in high viscosity immiscible fluid systems and application of static mixers as dispersion devices in such systems", *Chem. Eng. Commun.* **14**, 225-277 (1982).

8. Graebling, D., R. Muller, and J. F. Palierne, "Linear viscoelastic behavior of some incompatible polymer blends in the melt. Interpretation of data with a model of emulsion of viscoelastic liquids", *Macromolecules* **26**, 320-329 (1993).

9. Guido, S., and M. Villone, "Three-dimensional shape of a drop under simple shear flow", *J. Rheol.* **42**, 395-415 (1998).

10. Hobbie, E. K. and K. B. Migler, "Vorticity elongation in polymeric emulsions," *Phys. Rev. Lett.* **82**, 5393-5396 (1999).

11. Lerdwijitjarud, W., R. G. Larson, and A. Sirivat, "Influence of weak elasticity of dispersed phase on droplet behavior in sheared polybutadiene/ Poly(dimethylsiloxane) blends," *J. Rheol.* **47**, 37-57 (2003).

12. Lerdwijitjarud, W., A. Sirivat, and R. G. Larson, "Influence of dispersed-phase elasticity on steady state deformation and breakup of droplets in simple shearing flow of immiscible polymer blends," *J. Rheol* **48**, 843-862 (2004).

13. Levitt, L., C. W. Macosko and S. D. Pearson, "Influence of normal stress difference on polymer drop deformation", *Polym. Eng. Sci.* **36**, 1647-1655 (1996).

14. Luciani, A., M. F. Champagne, L. A. Utracki, "Interfacial tension coefficient from the retraction of ellipsoidal drops", *J. Polym. Sci. Pol. Phys.* **35**, 1393-1403 (1997).

15. Mighri, F., A. Ajji, and P. J. Carreau, "Influence of elastic properties on drop deformation in elongational flow", *J. Rheol.* **41**, 1183-1201 (1997).

16. Mighri, F., P. J. Carreau, and A. Ajji, "Influence of elastic properties on drop deformation and breakup in shear flow" *J. Rheol.* **42**, 1477-1490 (1998).

17. Mighri, F. and M. A. Huneault, "Dispersion visualization of model fluids in a transparent Couette flow cell," *J. Rheol.* **45**, 783-797 (2001).

18. Migler, K. B., "Droplet vorticity alignment on model polymer blends," *J. Rheol.* **44**, 277-290 (2000).

19. Milliken, W. J., and L. G. Leal, "Deformation and breakup of viscoelastic drops in plannar extensional flows", *J. Non-Newtonian Fluid Mech.*, **40**, 355-379 (1991).

20. Mo, H., C. Zhou, and W. Yu, "A new method to determine interfacial tension from the retraction of ellipsoidal drops", *J. Non-Newtonian Fluid Mech.* **91**, 221-232 (2000).

21. Palierne, J. F., "Linear rheology of viscoelatic emulsions with interfacial tension", *Rheol. Acta* **29**, 204-214 (1990).

22. Rumscheidt, F. D., and S. G. Mason, "Particle Motions in Sheared Suspensions. XII. Deformation and burst of fluid drops in shear and hyperbolic flow", *J. Coll. Sci.* **16**, 238-261 (1961).

23. Taylor, G. I., "The viscosity of a fluid containing small drops of another fluid", *Proc. R. Soc. London*, Ser. A **138**, 41-48 (1932).

24. Taylor, G. I., "The formation of emulsions in definable fields of flow", *Proc. R. Soc. London*, Ser. A **146**, 501-523 (1934).

25. Tretheway D. C., and L. G. Leal, "Deformation and relaxation of Newtonian drops in planar extensional flows of a Boger fluid" *J. Non-Newtonian Fluid Mech.* **99**, 81-108 (2001).

26. Varanasri, P. P., M. E. Ryan, and P. Stroeve, "Experimental study on the breakup of Model viscoelastic drops in uniform shear flow", *Ind. Eng. Chem. Res.* **33**, 1858-1866 (1994).

27. Wannaborworn S., M. R. Mackley, and Y. Renardy, "Experimental observation and matching numerical simulation for the deformation and breakup of immiscible drops in oscillatory shear," *J. Rheol* **46**, 1279-1293 (2002).

28. Wu, S., "Formation of Dispered phase in incompatible polymer blends-interfacial and rheological effects." *Polym. Eng. Sci.* **27**, 335-343 (1987).

29. Xing, P., M. Bousmina, and D. Rodrigue, "Critical experimental comparison between five techniques for the determination of interfacial tension in polymer blends: model system of polystyrene/polyamide-6", *Macromolecules* **33**, 8020-8034 (2000).

TABLES

Table I Polymers used

Polymers	Suppiers	M_n	Specific gravity
Low M_w PBd	General Electric International Operations Company Inc.	3,900	0.89
High M_w PBd	Aldrich Chemical Company, Inc.	702,000	1.2
PDMS	Chemical Innovation	91,700	0.976

Table II Effect of viscosity ratio

Blend systems	Blend components	T (°C)	Γ (mN/m)	G''_r	Wi_d	f (Hz)	τ_{rel} (sec)	τ_{osc} (sec)	Time scale ratio (τ_r)
A1	PBd/PDMS	67	3.85	0.16	0.0006-0.006	0.35	0.5	2.86	0.17
A2	PBd/PDMS	33	3.90	1.0	0.0034-0.034	0.1	1.5	10.0	0.15
A3	PBd/PDMS	20	3.94	3.0	0.0092-0.092	0.04	3.6	25.0	0.14

Table III Effect of time scale ratio ($\tau_r = \tau_{rel}/\tau_{osc}$)

Blend system	T (°C)	Γ (mN/m)	G''_r	W_{id}	f (Hz)	τ_{rel} (sec)	τ_{osc} (sec)	Time scale ratio (τ_r)
A2	33	3.90	1.0	0.0034-0.034	0.10	1.5	10.0	0.15
A2	33	3.90	1.0	0.0045-0.045	0.30	1.5	3.33	0.45
A2	33	3.90	1.0	0.0057-0.057	0.52	1.5	1.90	0.79

Table IV Effect of elasticity ratio

Blend system	Blend Components	T (°C)	Γ (mN/m)	G''_r	Wi_d	f (Hz)	τ_{rel} (sec)	τ_{osc} (sec)	Time scale ratio (τ_r)
A2	PBd /PDMS	33	3.90	1.0	0.0034-0.034	0.1	1.5	10.0	0.15
B1	0.02% High PBd Sol^n /PDMS	27	3.94	1.0	0.006-0.068	0.099	1.8	10.1	0.18
B2	0.05% High PBd Sol^n /PDMS	25	4.09	1.0	0.018-0.186	0.087	1.7	11.5	0.15

FIGURE CAPTIONS

Figure 1 G' vs. frequency at various temperatures:

(a) dispersed phases (pure PBd, 0.02% high M_w PBd sol^n and 0.05% high M_w PBd sol^n) strain = 80% at frequency 0.1-1 rad/s, strain = 20 % at frequency 1-100 rad/s; (b) matrix phases (PDMS 30M) strain = 80% at frequency 0.1-1 rad/s, strain = 20 % at frequency 1-100 rad/s.

Figure 2 G" vs. frequency at various temperatures:

(a) dispersed phases (pure PBd, 0.02% high M_w PBd sol^n and 0.05% high M_w PBd sol^n) strain = 80% at frequency 0.1-1 rad/s, strain = 20 % at frequency 1-100 rad/s ;(b) matrix phases (PDMS 30M) strain = 80% at frequency 0.1-1 rad/s, strain = 20 % at frequency 1-100 rad/s.

Figure 3 (a) G'_r at various temperatures, (b) G''_r at various temperatures.

Figure 4 Droplet deformation of blend system A2 at various times in one cycle at strain = 70 %, frequency = 0.1 Hz, $G''_r = 1$, $\tau_r = 0.15$, T = 33 °C, $Wi_d = 0.0238$, $d_o \sim 200$ μm and gap 2,200 μm.

Figure 5 Deformation parameters vs. time of blend system A2 at strain = 70%, frequency = 0.1 Hz, τ_r = 0.15, G''_r = 1, d_o = 200 μm, gap = 2200 μm: a) a* vs. time; b) c vs. time; c) Def* vs. time.

Figure 6 Amplitude of deformation parameters vs. Ca_m at d_o ~ 200 μm, gap = 2,200 μm : system A1, τ_r= 0.17, T = 67 °C, G''_r = 0.16, G'_r = 0.12, $Re_{osc} = 7.36*10^{-6}$; system A2, τ_r= 0.15, T = 33 °C, G''_r = 1.0, G'_r = 1.0, $Re_{osc} = 6.081*10^{-8}$; system A3, τ_r= 0.14, T = 20 °C, G''_r = 3.0, G'_r = 3.0, $Re_{osc} = 2.65*10^{-10}$, distance of drop from the center of plate ~ 6.8 mm. a) δa* vs. Ca_m; b) δc vs. Ca_m; c) δDef* vs. Ca_m.

Figure 7 Amplitudes of deformation parameters vs. Ca_m of system A2 at T = 33 °C, d_o = 200 μm, gap = 2,200 μm: frequency = 0.1 Hz, τ_r = 0.15; frequency = 0.3 Hz, τ_r = 0.45; frequency = 0.5 Hz, τ_r = 0.79, distance of drop from the center of plate ~ 6.8 mm. a) δa* vs. Ca_m; b) δc vs. Ca_m; c) δDef* vs. Ca_m.

Figure 8 Amplitudes of deformation parameters vs. Ca_m at G''_r = 1, d_o ~ 200 μm, gap = 2200 μm: system A2 (PBd/PDMS), τ_r = 0.15, T = 33 °C, frequency = 0.1 Hz; system B1(0.02 % high Mw PBd sol[n]/PDMS), τ_r = 0.18, T = 27 °C, frequency = 0.099 Hz; and system B2 (0.05% high Mw PBd sol[n]/PDMS), τ_r = 0.15, T= 25 °C, frequency = 0.1 Hz. a) δa* vs. Ca_m; b) δc vs. Ca_m; c) δDef* vs. Ca_m.

Figure 9 Droplet breakup of system A1, $G''_r = 0.16$, at strain amplitude of 558 %, $Ca_c = 1.5$, frequency = 0.05 Hz, $\tau_r = 0.019$, T = 67 °C, $d_o \sim 150$ μm and gap 2,200 μm.

Figure 10 Droplet breakup of system A1, $G''_r = 0.16$, at strain amplitude of 490 %, $Ca_c = 4.1$, frequency = 0.30 Hz, $\tau_r = 0.114$, T = 67 °C, $d_o \sim 150$ μm and gap 2,200 μm.

Figure 11 Critical capillary number vs. τ_r of system A1 (PBd/PDMS) at T = 67 °C, $G''_r = 0.16$ $d_o \approx 150$ μm, gap = 2,200 μm.

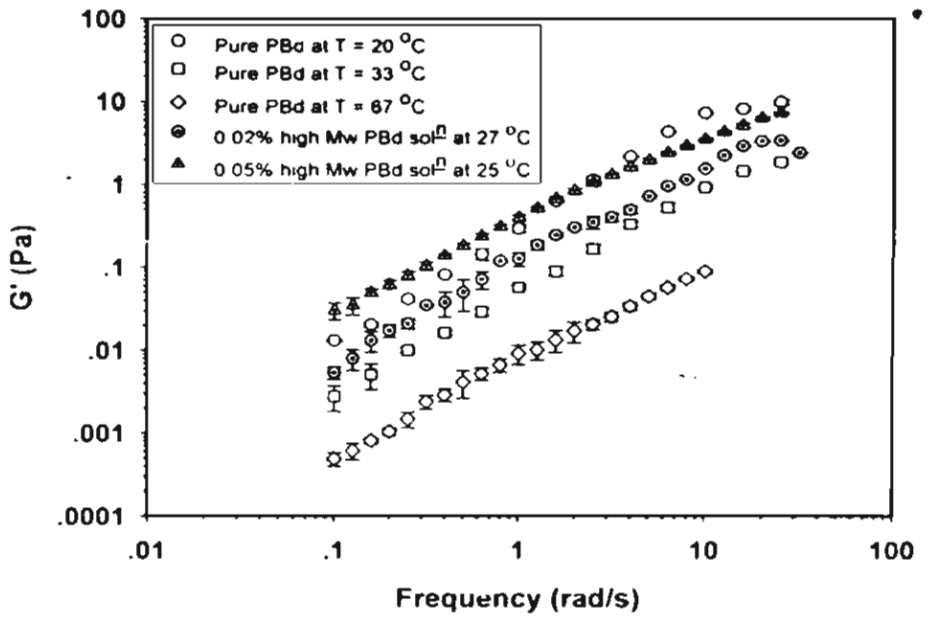
Pure PBd at T = 20 °C
Pure PBd at T = 33 °C
Pure PBd at T = 67 °C
0.02% high Mw PBd soln at 27 °C
0.05% high Mw PBd soln at 25 °C
G' (Pa)
Frequency (rad/s)
100
10
1
.1
.01
.001
.0001
.01
.1
1
10
100

(a)

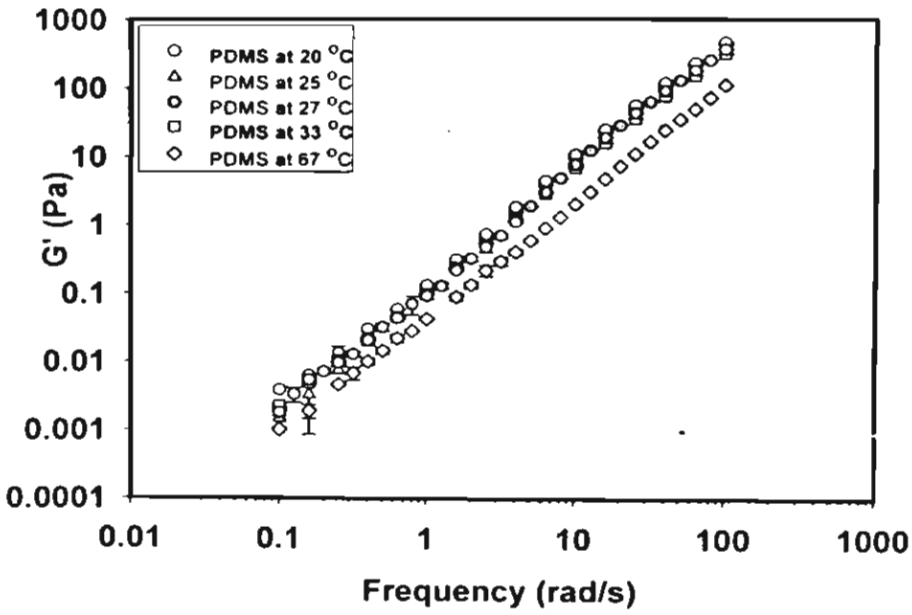
PDMS at 20 °C
PDMS at 25 °C
PDMS at 27 °C
PDMS at 33 °C
PDMS at 67 °C
G' (Pa)
Frequency (rad/s)
1000
100
10
1
0.1
0.01
0.001
0.0001
0.01
0.1
1
10
100
1000

(b)

Figure 1

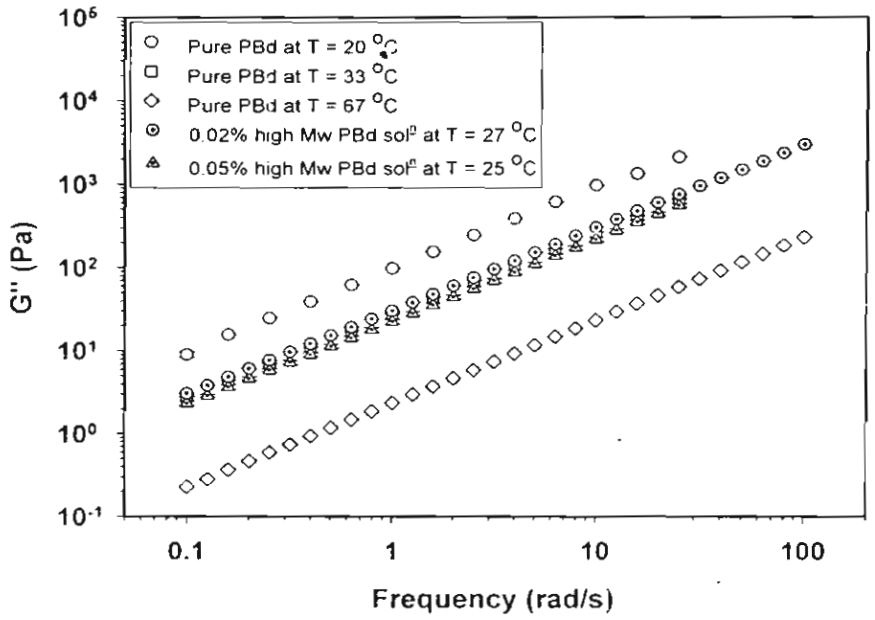
Pure PBd at T = 20 °C
Pure PBd at T = 33 °C
Pure PBd at T = 67 °C
0.02% high Mw PBd soln at T = 27 °C
0.05% high Mw PBd soln at T = 25 °C
G'' (Pa)
Frequency (rad/s)

(a)

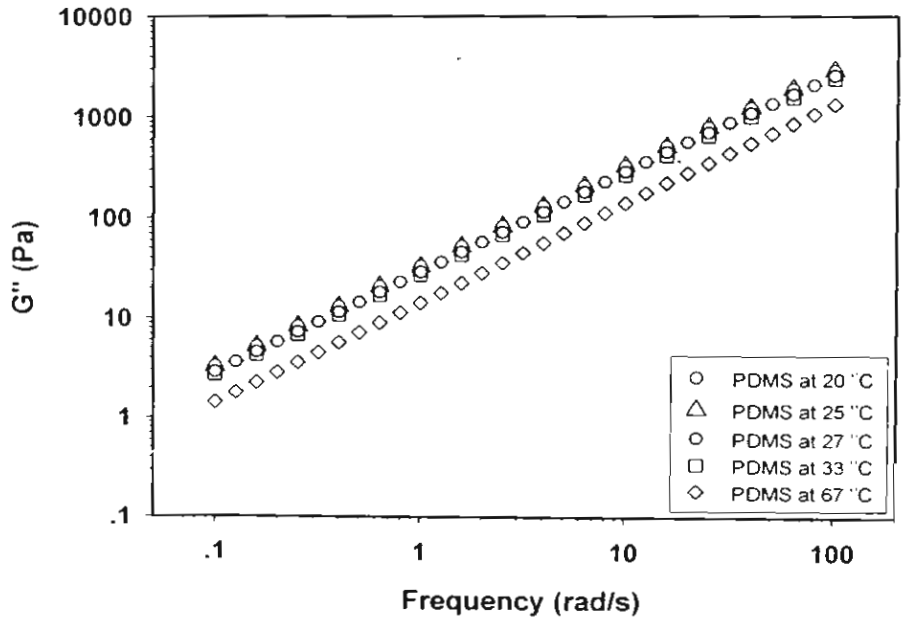
PDMS at 20 °C
PDMS at 25 °C
PDMS at 27 °C
PDMS at 33 °C
PDMS at 67 °C
G'' (Pa)
Frequency (rad/s)

(b)

Figure 2

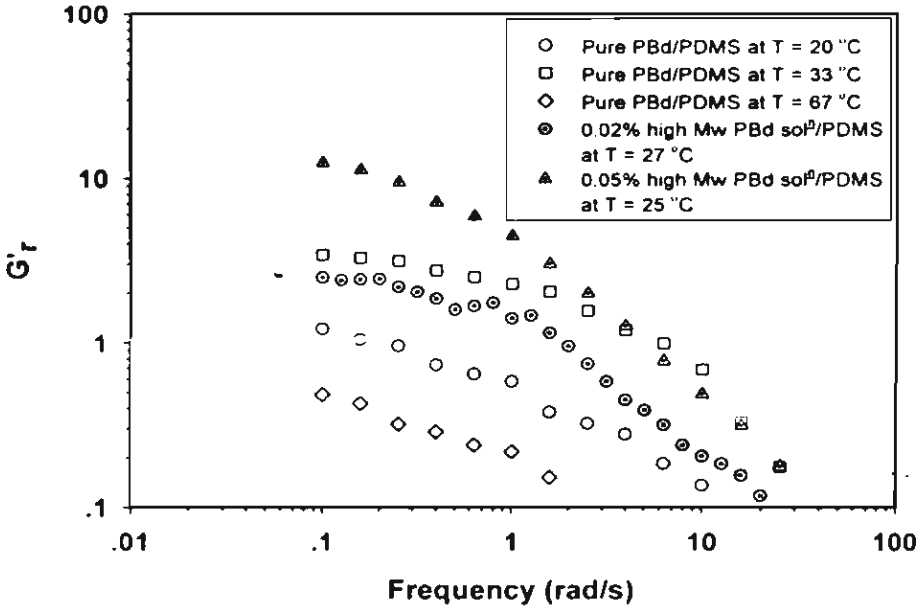
100
10
1
.1
G'r
.01
.1
1
10
100
Frequency (rad/s)
Pure PBd/PDMS at T = 20 °C
Pure PBd/PDMS at T = 33 °C
Pure PBd/PDMS at T = 67 °C
0.02% high Mw PBd sol/PDMS at T = 27 °C
0.05% high Mw PBd sol/PDMS at T = 25 °C

(a)

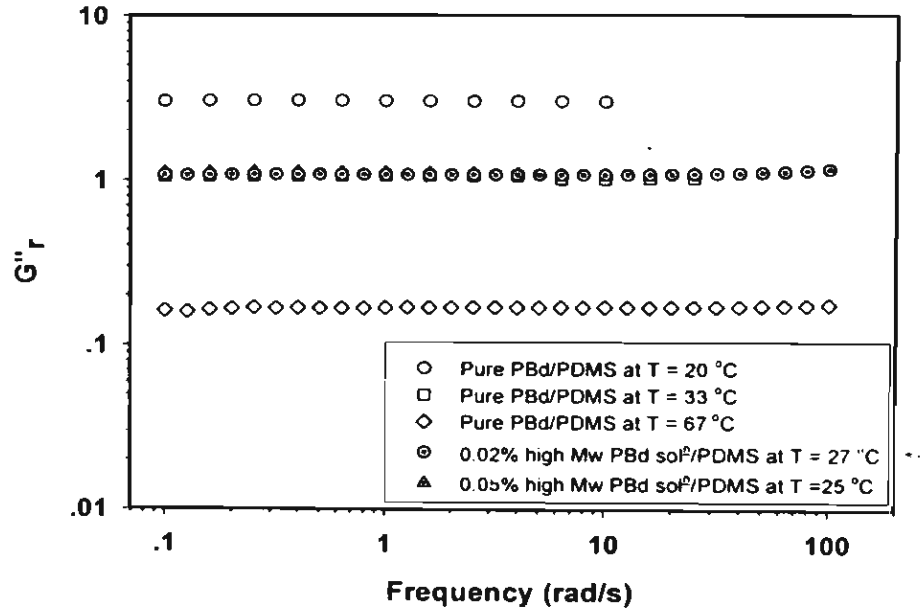
10
1
.1
.01
G"r
.1
1
10
100
Frequency (rad/s)
Pure PBd/PDMS at T = 20 °C
Pure PBd/PDMS at T = 33 °C
Pure PBd/PDMS at T = 67 °C
0.02% high Mw PBd sol/PDMS at T = 27 °C
0.05% high Mw PBd sol/PDMS at T =25 °C

(b)

Figure 3

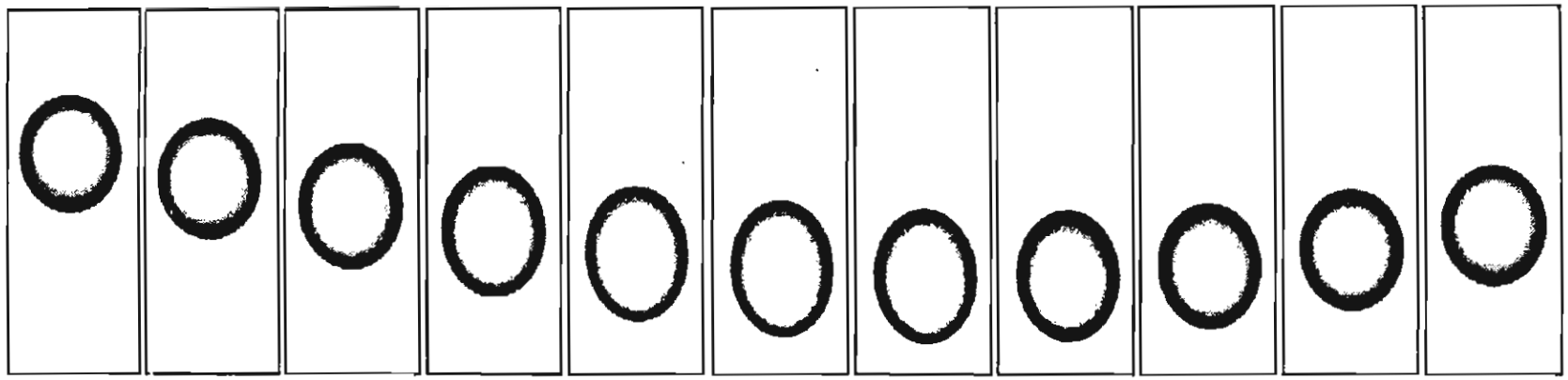

Time/τ_{osc}	0	0.05	0.10	0.151	0.201	0.251	0.301	0.35	0.401	0.45	0.501

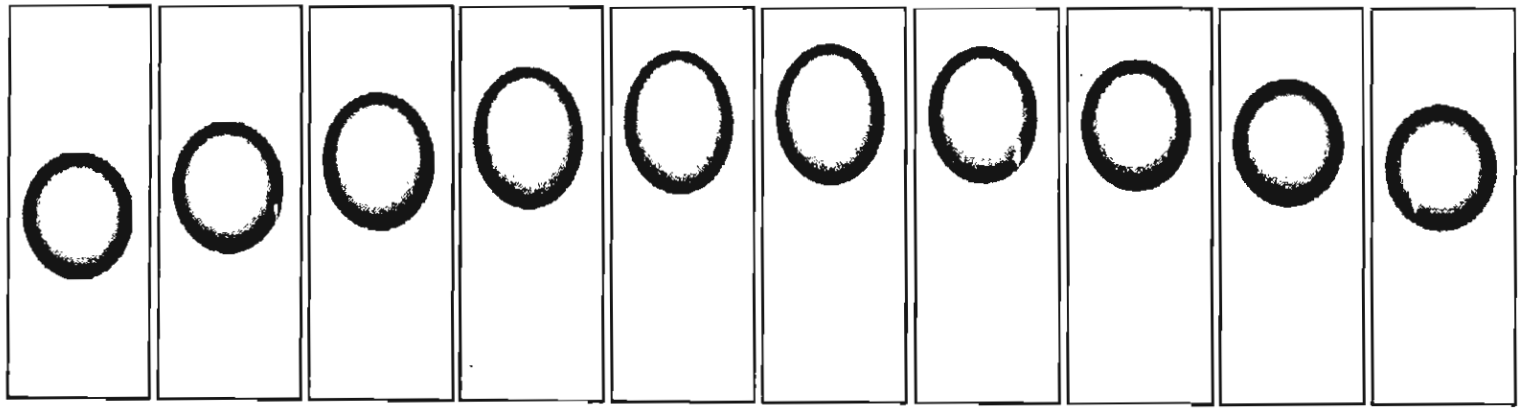

Time/τ_{osc}	0.55	0.6	0.65	0.701	0.75	0.801	0.851	0.901	0.95	1.0

Figure 4

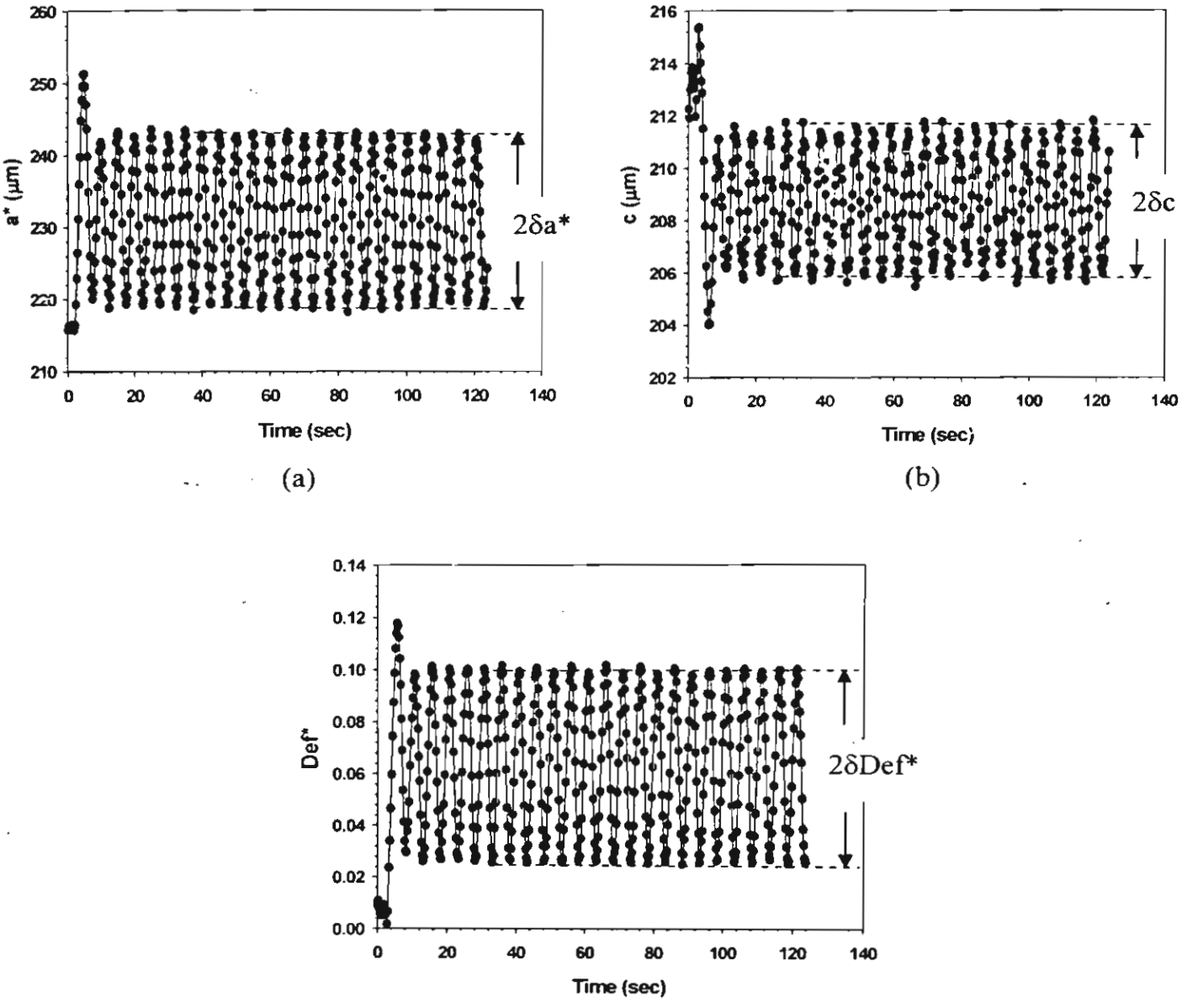

(a) (b)

(c)

Figure 5

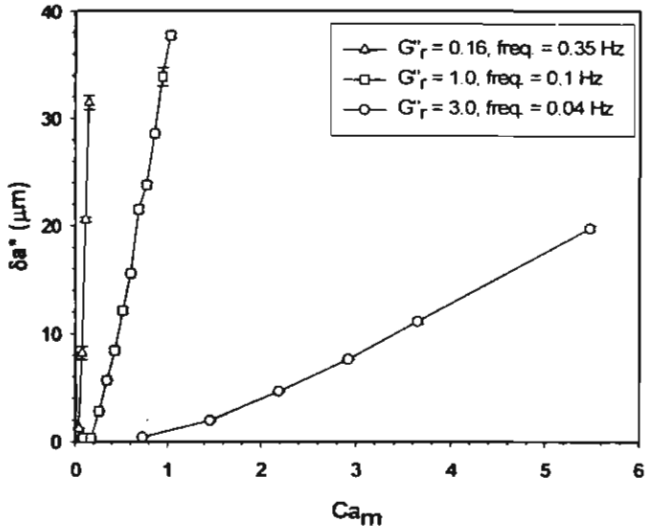
δa* (μm)
Ca_m
G''r = 0.16, freq. = 0.35 Hz
G''r = 1.0, freq. = 0.1 Hz
G''r = 3.0, freq. = 0.04 Hz

(a)

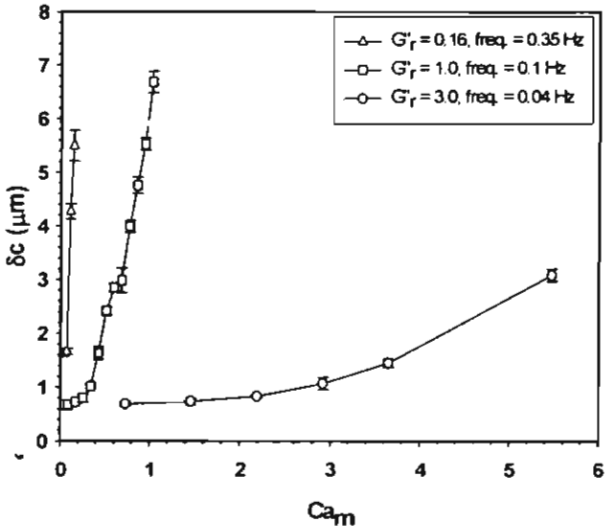
δc (μm)
Ca_m
G''r = 0.16, freq. = 0.35 Hz
G''r = 1.0, freq. = 0.1 Hz
G''r = 3.0, freq. = 0.04 Hz

(b)

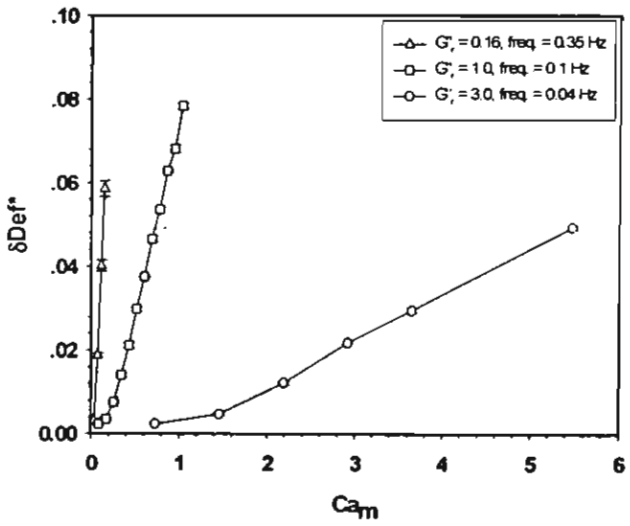
δDef*
Ca_m
G''r = 0.16, freq. = 0.35 Hz
G''r = 1.0, freq. = 0.1 Hz
G''r = 3.0, freq. = 0.04 Hz

(c)

Figure 6

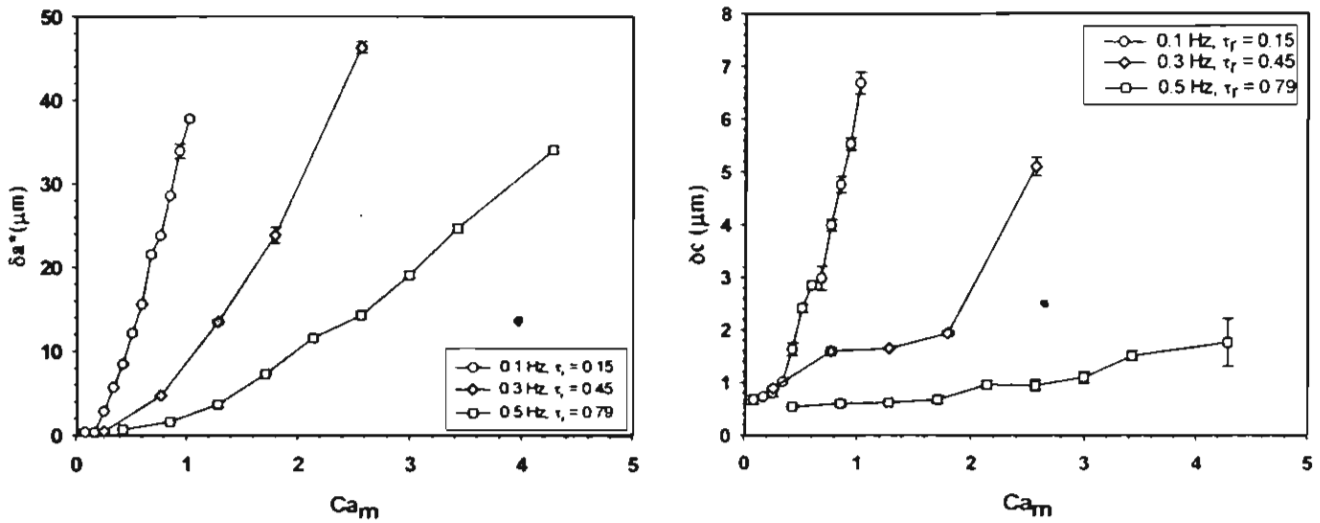
δa*(μm)
Ca_m
0.1 Hz, τ_f = 0.15
0.3 Hz, τ_f = 0.45
0.5 Hz, τ_f = 0.79

(a)

δc (μm)
Ca_m
0.1 Hz, τ_f = 0.15
0.3 Hz, τ_f = 0.45
0.5 Hz, τ_f = 0.79

(b)

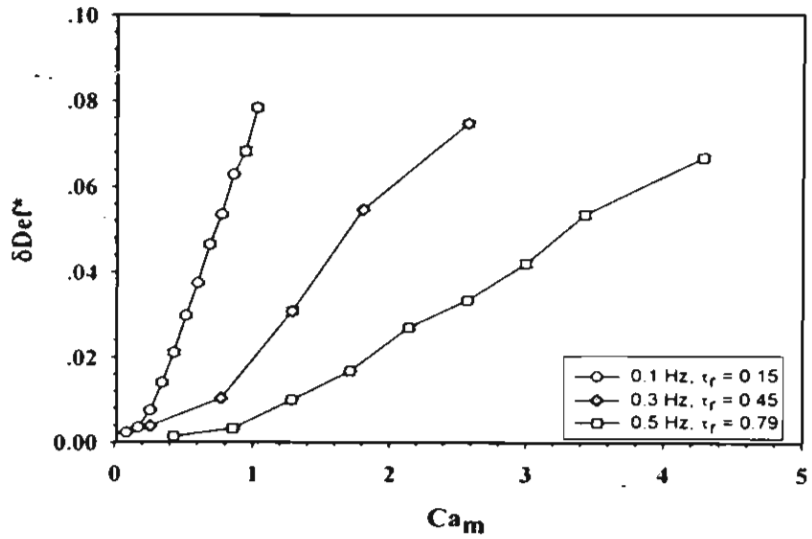
δDef*
Ca_m
0.1 Hz, τ_f = 0.15
0.3 Hz, τ_f = 0.45
0.5 Hz, τ_f = 0.79

(c)

Figure 7

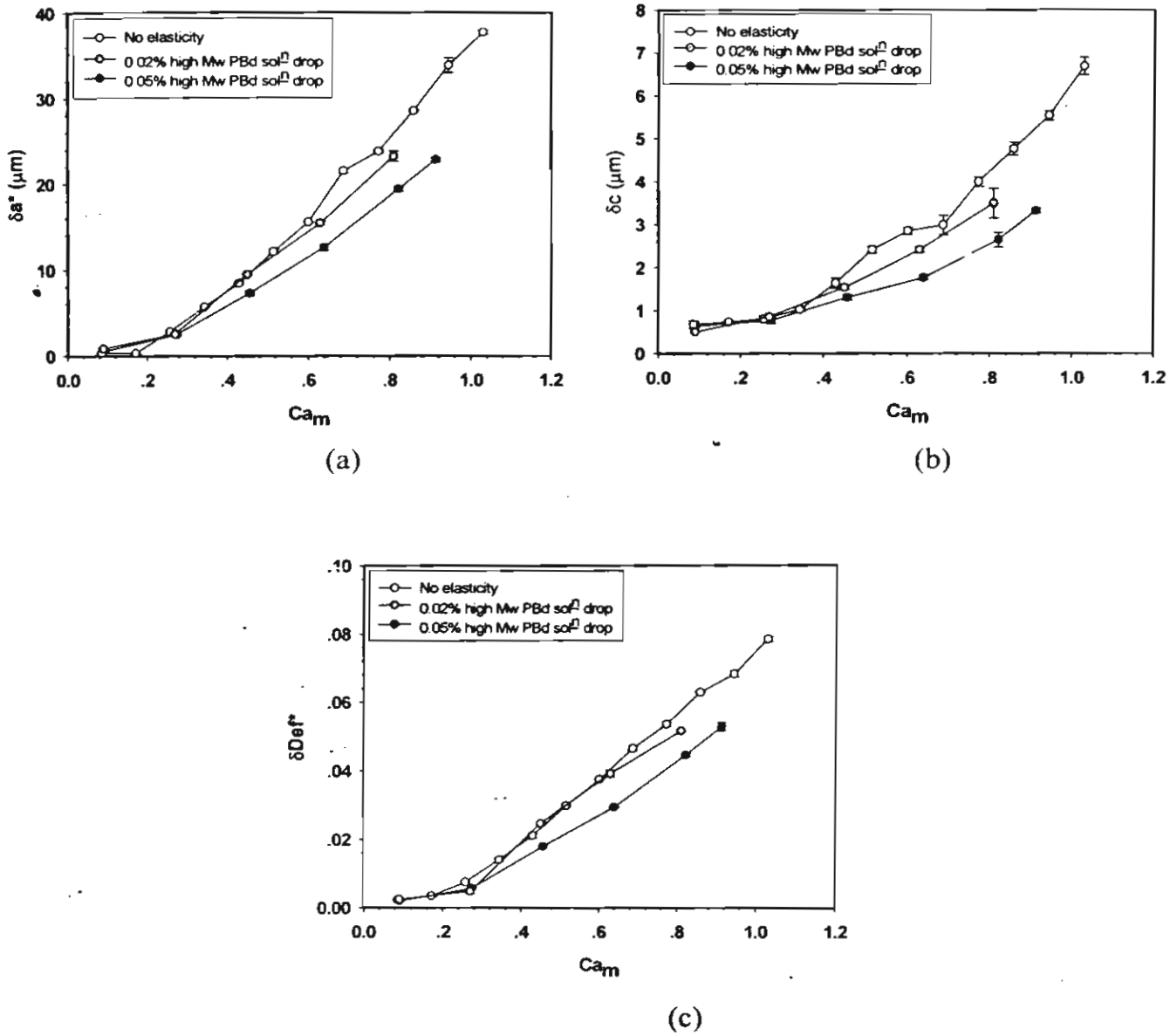
No elasticity
0.02% high Mw PBd sol drop
0.05% high Mw PBd sol drop
δa* (μm)
δc (μm)
δDef*
Ca_m
(a)
(b)
(c)

Figure 8

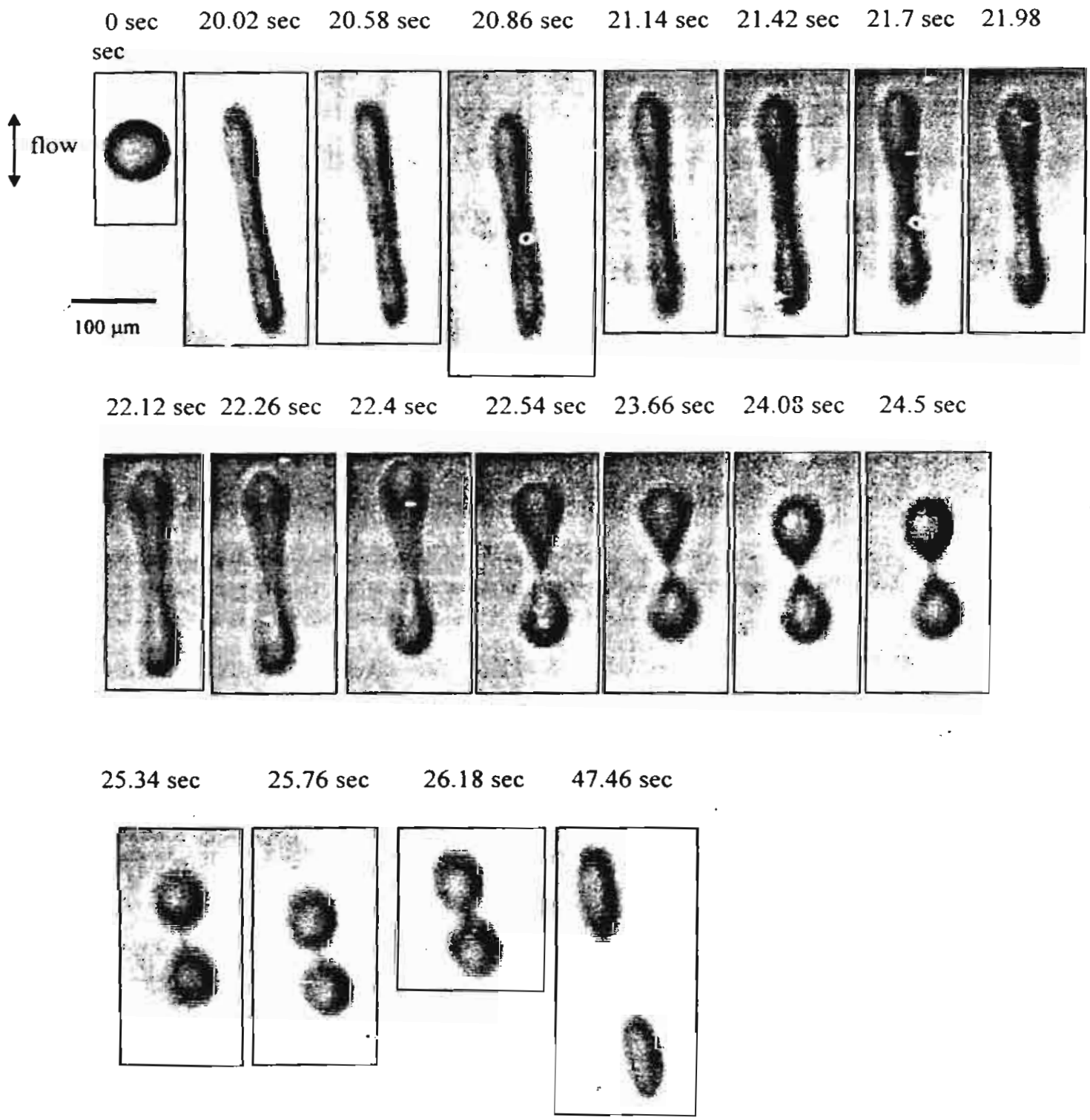
0 sec
20.02 sec
20.58 sec
20.86 sec
21.14 sec
21.42 sec
21.7 sec
21.98 sec
flow
100 µm
22.12 sec
22.26 sec
22.4 sec
22.54 sec
23.66 sec
24.08 sec
24.5 sec
25.34 sec
25.76 sec
26.18 sec
47.46 sec

Figure 9

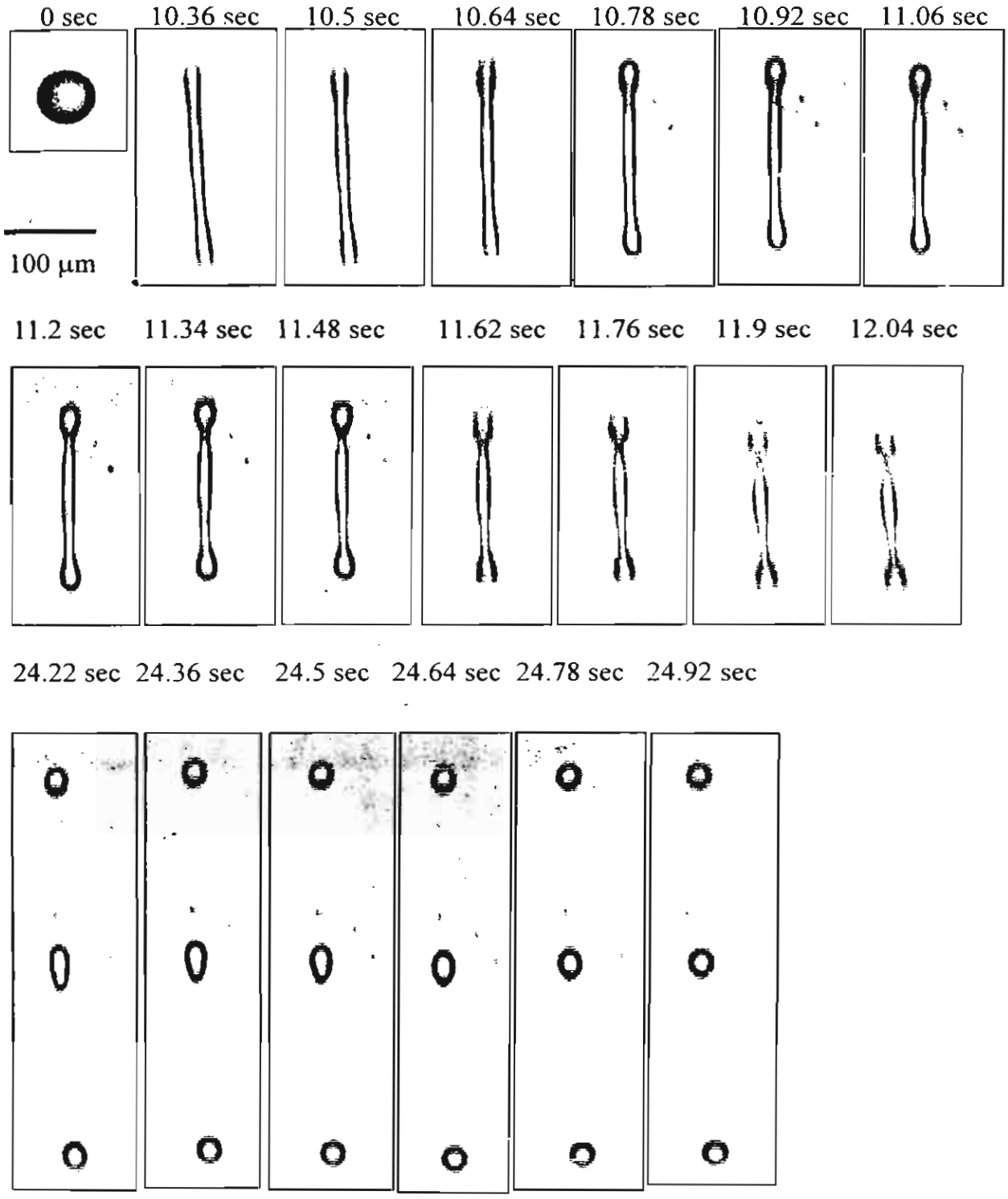
0 sec
10.36 sec
10.5 sec
10.64 sec
10.78 sec
10.92 sec
11.06 sec
100 μm
11.2 sec
11.34 sec
11.48 sec
11.62 sec
11.76 sec
11.9 sec
12.04 sec
24.22 sec
24.36 sec
24.5 sec
24.64 sec
24.78 sec
24.92 sec

Figure 10

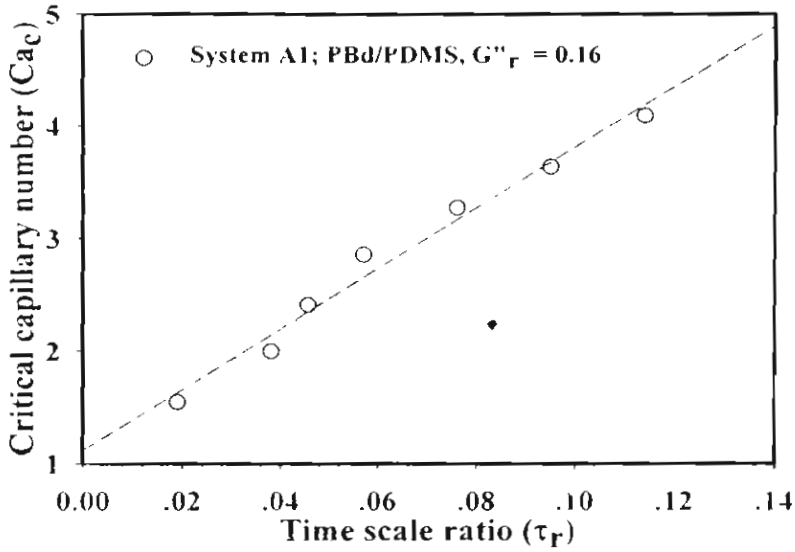
System A1; PBd/PDMS, G"r = 0.16
Critical capillary number (Cac)
Time scale ratio (τr)
1
2
3
4
5
0.00
.02
.04
.06
.08
.10
.12
.14

Figure 11

Chapter 2: Drop Deformation and Breakup in PS/HDPE Blends under Oscillatory Shear Flow

Anuvat Sirivat [a, *], Sakchai Patako [a], and Wanchai Lerdwijitjarud [b]

[a] Conductive and Electroactive Research Unit, Petroleum and Petrochemical College, Chulalongkorn University, Bangkok 10330, Thailand

[b] Department of Materials Science and Engineering, Faculty of Engineering and Industrial Technology, Silpakorn University, Nakhon Pathom 73000, Thailand

* Corresponding author: anuvat.s@chula.ac.th

Tel: 662 218 4131; Fax: 662 611 7221

Drop Deformation and Breakup in PS/HDPE Blends under Oscillatory Shear Flow

Abstract

Drop deformation and breakup in PS/HDPE viscoelastic melt blends were investigated under the effects of viscosity ratio, the time scale ratio and droplet elasticity under oscillatory shear flow using an optical flow cell. The deformation was studied in term of deformation parameters, $Def^* = a^*-c\ /a^*+c$ where a^* and c are the apparent drop principal axes and the minor axes of the droplets as measured from the time series of images. Amplitudes of deformation parameters are defined as the difference between the maximum and minimum values divided by two. The amplitudes increased linearly at small capillary number and nonlinearly at large capillary number, where the capillary is defined as the ratio between the matrix viscous force and the interfacial tension force. The deformation amplitude parameters decreased with increasing viscosity ratio, time scale ratio, and elasticity at any fixed capillary number. Drop breakup patterns observed were the non symmetric one-end tearing pattern for the system with a lower viscosity ratio, and the two-ends stretching and twisting for the system with a higher viscosity ratio. The critical capillary number increased with viscosity ratio but varied slightly with the time scale ratio.

I. INTRODUCTION

The investigation of deformation and breakup of an isolated Newtonian droplet in an immiscible Newtonian matrix was first pioneered by Taylor (1932, 1934). He observed that droplet deformation and breakup of isolated droplets in a Newtonian blend under quasi-steady conditions (i.e., gradually increasing deformation rate) are controlled by two dimensionless parameters. The first parameter is the viscosity ratio (η_r), which is the ratio between the viscosity of the dispersed phase (η_d) to that of the matrix phase (η_m):

$$\eta_r = \eta_d / \eta_m \tag{1}$$

The second parameter is the capillary number (Ca), which is the ratio of matrix viscous stress to interfacial stress:

$$Ca = \frac{D_o \gamma \eta_m}{2\Gamma} \tag{2}$$

where $\gamma \eta_m$ is the viscous shear stress, with γ is the shear rate and η_m the matrix viscosity, D_o is initial droplet diameter, and Γ is the interfacial tension.

Taylor predicted that the deformation parameter, Def, depending on Ca and η_r, is given by

$$Def \equiv \frac{a-b}{a+b} = Ca\frac{19\eta_r + 16}{16\eta_r + 16} \tag{3}$$

where a and b are lengths of the major and minor axes of the deformed droplet, respectively. Taylor also predicted that the critical point at which the viscous force overcomes the interfacial force leading to droplet breakup occurs at $Ca_c \approx 0.5$ and $Def_c \approx 0.55$ for a steady (or quasi-steady, if the flow rate is very slowly increased) simple shearing flow with a viscosity ratio of around unity. Ca_c is a minimum when η_r is around unity [Grace (1982); De Bruijn (1989)]. For viscosity ratios near unity, the steady-state three-dimensional shape of an isolated deformed Newtonian droplet sheared in a Newtonian matrix can be represented by an ellipsoid having three different principal axes, in which the steady-state length of the minor axis of the ellipsoid in the vorticity direction was larger than that in the shear-gradient direction. The major axis of deformed droplet orients at an angle θ with respect to the flow direction, (Guido and Villone 1998).

The breakup condition for extensional flows differs from that for shearing flows; for general two dimensional incompressible flows droplet breakup is also controlled by the flow-type parameter, α, which is zero for shearing flow and unity for planar extensional flow [Rallison and Acrivos (1978), Bentley and Leal (1986)].

Elasticity of the droplet and/or matrix phase in binary blend of viscoelastic fluids should be an important factor influencing the droplet deformation and breakup. The behaviors of droplet under a flow field for immiscible viscoelastic blends have been investigated [Flumerfelt (1972); Elmendrop and Maalcke (1985); Wu (1987); Milliken

Capillary number over finite ranges. Droplet viscosity and elasticity generally impeded breakup under oscillatory shear. Critical capillary number for breakup, the number of resultant daughter droplets, and the number of cycle required for breakup to occur increased with the time scale ratio. The apparent breakup pattern changed from the dumbbell type to the end-pinching type as time scale ratio increased.

In our work reported below, we take a further step towards understanding the behaviors of commercial blends by using highly elastic polymer melts for both the droplet phase and the matrix phase. The oscillatory droplet deformation and the breakup were studied. The effect of the viscosity ratio (0.58, 0.12. and 0.06), the effect of time scale ratios (4.0, 16.6, 33.2 and 63.8), and the effect of the elasticity were investigated by using a flow cell mounted on an optical microscope where the deformation and various distinct breakup patterns of isolated droplets in oscillatory shear were first observed.

II. EXPERIMENTS

A. Materials

The materials used in this study were high-density polyethylene (HDPE) as the matrix phase and polystyrenes (PS) as the droplet phases, respectively (suppliers and grades are tabulated in Table I). Polystyrene grades were obtained from the manufacturers in the form of flake; they were crushed and size-selected by passing the flakes through a 425 μm sieve. To eliminate any possible volatile components, all polymers were heated at around 80°C under vacuum for 12 hours. The polymer blend systems and their experimental conditions are listed in Tables II - IV. The interfacial tension values for the polymer blend systems used in this work were taken from the literature [Brandrup and Immergut (1989)].

B. Rheological Characterization

Each polymer was molded into a disk, 25 mm in diameter and 1 mm thick by using a compression mold (Wabash, model V50H-18-CX) at 145°C for HDPE1, and at 135°C for PS1, PS2, and PS3. We used a cone-and-plate rheometer (Rheometrics Scientific: Model ARES, 25-mm plate diameter with cone angle 0.1 rad) to measure the dynamic storage modulus (G') and the dynamic loss modulus (G") of each polymer. The rheological properties were obtained at frequencies between 0.1 and 100 rad/s using the dynamic frequency sweep test mode (strain control). From the rheological properties of pure polymers at various temperatures, the desired pairs of polymers and operating

temperatures were selected for further study. The rheological properties are shown in Fig. 1. In this study, we investigated the effect of viscosity ratio at G" ratios equal to 0.58, 0.12 and 0.06 (systems A1, A2, A3) at a fixed time scale ratio equal to 32. We investigated system A4 at a fixed G" ratio of unity at time scale ratios equal to 4, 16.6, 33.2 and 63.8; the time scale ratio was varied by varying frequencies. Different grades of PS were used to study the effect of droplet elasticity; they are tabulated in Table IV.

C. Observations of an Isolated Droplet in Shearing Flow

1. Oscillating Shear Apparatus

To generate oscillatory shear and to observe droplet deformations, we used a flow cell device (Linkam CSS 450, Linkam Scientific Instruments Ltd., UK) consisting of two transparent quartz parallel disks mounted on an optical microscope (Leica DMRPX, Leica Imaging Systems LTd., Cambridge, England), and connected to a CCD camera (Cohu 4910, Cohu Inc., CA). The images were recorded by a CCD camera, and they were analyzed on a computer using the Scion Image software.

2. Sample Preparation

HDPE used as the matrix polymer was molded into a disk 25 mm in diameter and 0.5-1 mm thick by compression molding. Various PS droplets were introduced into the matrix by using a pin to insert a small amount of PS powder on a HDPE disk, and it

was covered with another HDPE disk to form a sandwich. The sandwich was placed on the bottom quartz disk, which was then covered with the top quartz disk. The sample was held at the temperature until complete melting occurred.

3. Determination of Relaxation Time

The sample was inserted between the two quartz disks of the flow cell. The sample was heated to the temperature chosen for the measurement. A desired strain was imposed onto a selected drop. The drop then was allowed to relax into a spherical shape. Deformation of the ellipsoidal droplet was observed using an optical microscope with 5 – 10 frames/second for a total of 300 images.

Using the optical microscope, the droplet images were captured only from the top view, i.e., a view containing the flow and vorticity directions. Since only a projection of the droplet onto the flow-vorticity plane can be imaged from this view, this view cannot determine the true lengths of the principal axes (a, b, and c: figure 1), because two of them, a and c (those in the flow and the shear-gradient directions), are not parallel to the flow and shear gradient directions. However, the lengths of these axes can be determined by using the affine angle of rotation of the droplet in the plane containing the flow and shear-gradient directions together with the condition of volume preservation, $D_o^3 = abc$ [Almusallam *et al.* (2000)]. Although the lengths of the principal axes can be approximated by using the method mentioned above, we adopted to use the lengths of the observable axes, as shown in Figure 1, to describe the behavior of each droplet. Thus, we define a modified deformation parameter Def* as:

$$Def^* \equiv \frac{a^* - c}{a^* + c} \tag{4}$$

where the asterisk denotes that the deformation parameter is an apparent one obtained from the droplet image projected onto the flow-vorticity plane, as shown in Figure 1. The deformation parameter, Def*, of a retracting droplet vs. time was measured; it is known to decay exponentially [Lucinia *et al.* (1997)] in the form of the following equation:

$$Def^* = Def^*_o \exp[-t/\tau_{rel}] \tag{5}$$

The slope of Def^*/Def^*_o vs. t on a semi-log plot is simply the characteristic relaxation time for a single isolated drop. To ensure the characteristic relaxation time of single drop studied from the small deformation did not depend on the strain, the relaxation time experiments were carried out at various strain units (1%, 2%, 5% and 10%) at the same shear rate of 1.0 s^{-1}. The characteristic time scale ratio was calculated from the ratio of the relaxation time and the oscillation time ($\tau_r = \tau_{rel} / \tau_{osc}$).

4. Oscillatory Shear Deformation

This experiment is similar to the relaxation experiment, where the HDPE matrix phase was loaded into the flow cell and various PS droplets were subsequently inserted into the matrix by using a pin to put a small amount of PS powder on a HDPE disk. The sample was heated to a desired temperature and gap. Before we started each

experiment, the drop was allowed for relax until it retained a spherical shape. Appropriate strain and frequency were then applied. Since the shearing mode was sinusoidal oscillatory the Linkham device, which has one stationary and one moving plate, inevitably caused the droplet move back and forth. For a given frequency, we increased the strain in order to vary Ca_m up to a strain in which we could no longer capture all drop images during a deformation cycle. In a given droplet deformation experiment, six hundred to seven hundred images were recorded; for each period of deformation the number of captured images was equal to or above 32 in order to track the deformation time series in details. The droplet deformation parameters, i.e. the major and minor axes, were measured as functions of time, frequency, strain, G" ratio, and G' ratio.

III. RESULTS AND DISCUSSION

A. Rheological Characterization

The rheological property of the blend components was obtained from the melt rheometer (ARES, Rheometrics Scietific, Ltd.). Figures 2 and 3 show the storage modulus (G') and the loss modulus (G"), respectively. The data indicate that the two polymers behave as Maxwell fluids since the slope of G' is approximately equal to two, and the slope of G" is approximately equal to one. G' and G" both vary with temperature; both functions decrease with increasing temperature. Polystyrene has a higher temperature-dependent viscosity than that of high-density polyethylene, allowing

us to obtain the desired G' and G" values by adjusting the operating temperature. The values of the G' and G" ratios of all blend systems studied are shown in Figure 4.

B. Relaxation Experiment

The relaxation time scale of each blend studied was obtained from a step strain experiments performed at various shear rates and drop sizes. The characteristic relaxation time scales were then determined and obtained only from the ranges of shear rates and drop size in which the time scales were nearly constant. The characteristic relaxation times were 290 sec, 220 sec, 180 sec and 332 sec, for PS2/HDPE1 blends with $G"_r$ equal to 0.58, 0.12, 0.06 and 1, respectively (Tables II and III). The characteristic relaxation times are 670 sec and 105 sec for PS3/HDPE1 and PS1/HDPE1 blends, respectively, when $G"_r$ is equal to 0.12 (Table IV).

C. Oscillatory Shear Experiment

In this study, there are many parameters involved, we grouped them into dimensionless pi groups; they are Capillary Number (Ca_m), Reynolds number (Re), time scale ratio (τ_r), and Weissenberg number (Wi_d). Ca_m and Re are defined as:

$$Ca_m = \frac{G_m"(\omega)\gamma d}{\Gamma} \tag{6}$$

$$Re = \frac{\rho_d \omega^2 d^2}{G_d"(\omega)} \tag{7}$$

where γ is the imposed strain on the matrix, d is the diameter of droplet, $G_m''(\omega)$ is the loss modulus of the matrix phase, $G_d''(\omega)$ is the loss modulus of the disperse phase, ρ_d is the density of the disperse phase, and Γ is the interfacial tension between two polymers. The time scale ratio is defined as:

$$\tau_r = \tau_{rel}/\tau_{osc} \tag{8}$$

where τ_{rel} is the relaxation time scale obtained from the relaxation experiment, τ_{osc} is the period of oscillation, $\tau_{osc} = 1/f$, where f is the imposed oscillation frequency.

The Weissenberg number (Wi_d), a dimensionless number, is formally the ratio of the first normal stress difference to twice the shear stress at the imposed shear rate. It is defined in our oscillatory shear flow as

$$Wi_d = 2G'_d(\omega)/G''_m(\omega)\gamma \tag{9}$$

The values of the Weissenberg number for blend systems are shown in Tables II, III and IV : system A1 (G''_r = 0.58), Wi_d = 0.012 – 0.084; system A2 (G''_r = 0.12), Wi_d = 0.0052 – 0.031; system A3 (G''_r = 0.06), Wi_d = 0.0051 – 0.031; system A4 (G''_r = 1, τ_r = 4, 16.6, 33.2 and 63.8), Wi_d = 1.66 – 11.35; system B1 (G''_r = 0.12), Wi_d = 0.0014 – 0.0083; system C1 (G''_r = 0.12), Wi_d = 0.378 – 2.26 .We divide our work on droplet deformation into 3 parts: the effect of viscosity ratio, the effect of time scale ratio, and the effect of droplet elasticity. Finally, we investigated drop breakup patterns and determined the critical capillary numbers.

Figure 5 shows optical photographs of a droplet under sinusoidal oscillatory shear deformation: system A3, G''_r = 0.06, Ca_m = 35, τ_r = 32 The nominal spherical drop size was 180 μm. The droplet can be seen to stretch along the flow direction, to

retract to its original value, to stretch again, and finally to retract back when the cycle is complete, or when the observation time over the oscillatory time scale ratio is unity. No breakup was observed for this droplet even though G''_r was quite low. Ca values applied to the matrix and the disperse phase are 35 and 2.10, respectively. These values are well above the critical Ca_m values of Newtonian droplets in Newtonian matrices or viscoelastic droplets in viscoelastic matrices in steady state shear which vary between 0.5 and 1.0, depending on Wi_d [Lerdwijitjarud *et al.* (2003,2004)]. The large time scale ratio of 32 implies that the droplet did not have time to relax to attain equilibrium deformation at any particular instant. The apparent deformation observed probably comes from accumulated contributions from the previous stress history in a cycle. We may also note that the apparent droplet deformation in oscillatory shear as seen does not reflect the true deformation occurring, similar to but more complicated than that in steady shear, due to the combination of the droplet rotation and the periodic change in shear direction.

Figure 6 shows the deformation parameters, a*, c, and Def* vs. time for the droplet of system C1. In the steady state oscillatory shear deformation, we define the deformation amplitudes as the one halves of the differences between the maximum and the minimum vales of the corresponding deformation parameters: a*, c, and Def*, respectively. There is an initial transient period, of about 2-3 cycles, in which the deformation parameters (a*, c, and Def*) fluctuate but do not yet attain the final steady state oscillations. Beyond this initial period, we determined the steady state deformation amplitudes from the time series of the captured images.

Figures 7a, 7b, and 7c show the deformation amplitudes δa*, δc, and δDef* as functions of Ca_m for the three blend systems studied: system A1,G''_r = 0.58; system A2, G''_r = 0.12; and system A3, G''_r = 0.06. The corresponding relaxation time scales of these systems are 290 sec, 220 sec, and 180 sec, respectively. In these experiments, the oscillatory shear frequency was chosen to be 0.11 Hz, 0.15 Hz, and 0.18 Hz, respectively so that the corresponding time scale ratios are all identical and equal to 32 (Table II). We can see that, for a given Ca_m, Def* is greater for a droplet with a smaller viscosity ratio. This suggests that droplet viscosity resists the droplet oscillatory deformation, a similar finding to that of the steady state shear flow. For the blends systems A1-A3 studied, a*, c, and Def* appear to vary nonlinearly with Ca_m above certain values of Ca_m. Since a* and Def* are only apparent deformation parameters, due to the a* projection and the periodic droplet rotation, we adopt to identify the extent of linear oscillatory deformation from c, the minor axis observed. In Fig 7b, we can see that nonlinear deformation appears at Ca_m equal to 43 and 47 for the systems with G''_r equal to 0.06 and 0.12, respectively. The corresponding products of Ca_m and G''_r are 2.58 and 5.64, respectively. The product of Ca_m and G''_r can be identified as simply the ratio of the droplet viscous shear force over its interfacial tension. For the blend with G''_r equal to 0.06, we were unable to observe the nonlinearity. Thus, a lower droplet viscosity leads to larger deformation amplitudes as well as it allows the droplet to deform nonlinearly at a lower applied shear force at a given time scale ratio.

Figures 8a, 8b and 8c show the deformation amplitudes δa*, δc, and δDef* vs. Ca_m for system 4 at four different time scale ratios: τ_r = 4, 16.6, 33.2 and 63.8, as also

tabulated in Table III. In order to study the effect of time scale ratio on droplet oscillatory deformation, system A4 was chosen so that G''_r was fixed at unity and its relaxation time scale was 332 sec. The time scale ratio was varied by varying the imposed frequency: 0.12 Hz, 0.05 Hz, 0.10 Hz, and 0.192 Hz, respectively. The corresponding periods of oscillation are 83.3 sec, 20.0 sec, 10.0 sec, and 5.2 sec, respectively. For a given time scale ratio, capillary number was varied by varying strain, according to Eq. (6). The droplet sizes chosen were between 185-200 μm. Consequently, Wi_d also varied with strain (Eq. 9). But the variations of Wi_d with strain or Ca_m are nearly within the same ranges for the four time scale ratio experiments (Table III): the range of Wi_d is between 1.6 and 11.4. Therefore, the results of the four experiments (Table III) can be compared and used to determine the effect of time scale ratio. In Fig. 8b, we see that δc varies linearly with Ca_m up to certain values; the departure from deformation linearity occurs at Ca_m equal to 35, 26, and 15 for corresponding τ_r equal to 63.8, 33.2, and 16.6, respectively. This finding is opposite to our expectation where we expect that a smaller relaxation time scale, or a lower time scale ratio, would favor the affine deformation and linearity would be extended to high Ca_m values. However, we may refer to data in Table III that the variations of Wi_d in these experiments are quite large, and the droplet elasticity may have played a role.

Figures 9a, 9b and 9c show the amplitudes of the deformation parameters δa*, δc, and δDef* vs. Ca_m for three systems: the low elasticity systems A2 and B1, and the high elasticity system C1 (Table IV). The corresponding G'_r is equal to 0.002, 0.0-1, and

0.55, respectively. G''_r for the three systems is equal to 0.12, as chosen and adjusted by the operating temperatures. Since the time scale ratio was fixed at 32, the oscillatory frequency was chosen to be 0.048 Hz, 0.15 Hz, and 0.33 Hz for systems B1, A2, and C1, respectively. The corresponding relaxation time scales are 670 sec, 220, and 105 sec, respectively. As shown in these figures, at any given Ca_m the amplitudes of the deformation parameters generally decrease with increasing elasticity; this implies that the droplet elasticity also resists oscillatory shear deformation. We can observe that the amplitudes of the deformation parameters of the low elasticity systems A2 and B1 increase linearly with Capillary number up to about 20. For the highly elastic system C1, the deformation amplitude parameter c, as shown in Fig 9b, increases less than linearly at all Ca_m investigated up to about 200. In Fig 9b, it may be noted that the relation δc vs. Ca_m would intercept the x axis at a finite value of Ca_m equal to 20, in the limit of δc approaching zero. This intercept can be interpreted as the oscillatory yield stress required to deform this highly elastic droplet.

Figures 10 and 11 show optical micrographs of drop breakups under oscillatory deformation of systems A1 and A3 whose G''_r are 0.58 and 0.06 (Tables II and III), respectively. For both systems, we applied an oscillatory frequency of 0.20 Hz; the corresponding time scale ratios were 58 and 36, respectively.. The original drop sizes were 167 for system A1, and 173 μm for system A3. Wi_d numbers were of order 10^{-3}, and hence elasticity was negligible. The main difference is therefore the viscosity ratio: 0.58 for system A1, and 0.06 for system A3. In these two breakup experiments, drops were subjected to many cycles before breakups were observed. For system A1 of higher

viscosity ratio, the breakup occurred through the non-symmetric one-end tearing pattern which resulted in many daughter drops, as can be seen in Figure 10. For system A3 whose viscosity ratio was lower, the breakup occurred through a diamond shape formation, two-ends stretching and twisting which ultimately resulted in only few satellite drops at each end (Figure 11). The critical Capiilry numbers, Ca_c, were 102 and 93, respectively. We may presume that the twisting at both ends is presumably a result of low viscosity ratio. Other breakup patterns of system A1 and A3 at other time scale ratios were also observed which are similar to the two patterns shown in Figures 10 and 11.

Figures 12, 13 and 14 show the critical capillary number, the critical Weisenberg number, and the number of cycles required for drop breakups to occur as functions of the time scale ratio of the two systems A1 and A3. From Figure 12, we may note that the system of higher viscosity, A1, has a higher critical capillary number. Therefore, a larger shear force exerted by the matrix is required to break a drop with a higher viscosity. On the other hand, the critical capillary number varied slightly with the time scale ratio; notably it is higher as the time scale ratio approaches zero. This finding suggests that a larger shear force is required for a drop to breakup when it is closer to the equilibrium deformation state. Figure 13 shows that the corresponding Weisenberg number increases linearly with the time scale ratio; the dependence changes to a nonlinear one at large time scale ratio. This may be interpreted as follows; a drop whose deformation state is far away from its equilibrium deformation state requires a smaller shearing force from the matrix for a drop to breakup at a given droplet elasticity. Finally,

Figure 14 shows that the number of cycles required for drop breakup; it increases with the viscosity ratio and the time scale ratio. The first dependence seems obvious. On the other hand, the explanation for the second dependence is less clear.

IV. CONCLUSIONS

We observed the oscillatory deformations of droplets in PS/HDPE blends. In particular, we investigated three effects on droplet oscillatory deformation: the effect of viscosity ratio, the effect of time scale ratio, and the effect of droplet elasticity

At a given capillary number, amplitudes of deformation parameters decreased with increasing viscosity ratio, time scale ratio and elasticity. The dependences of the amplitudes on capillary number were linear at small values; whereas the dependences became nonlinear at large capillary number. Droplet viscosity and elasticity tend to disrupt the affine oscillatory deformation, whereas a higher time scale ratio promotes the affine deformation.

The deformed droplet with little relaxation appears to be easier to break. The drop breakup patterns were the non symmetric one-end tearing and breaking pattern for the high viscosity ratio system, and the two-ends stretching and twisting pattern for the lower viscosity ratio system. The critical capillary number increased with viscosity ratio but varied slightly with the time scale ratio.

V. ACKNOWLEDGEMENTS

AS would like to acknowledge the fund from TRF, grant no. BRG 4680015, and the fund from Conductive and Electroactive Research Unit; Chulalongkorn University. Kindly help for manuscript preparation from Prof. Ronald G. Larson is gratefully acknowledged.

REFERENCES

1. Almusallam A. S., R. G. Larson, and M. J. Solomon, "A constitutive model for the prediction of ellipsoidal droplet shapes and stresses in immiscible blends", *J. Rheol* **44**, 1055-1083 (2000).
2. Bentley, B.J., and L. G. Leal, "An experimental investigation of drop deformation and breakup in steady, two-dimensional linear flows," *J. Fluid Mech.*, **167**, 241-283 (1986).
3. Brandrup, J. and E. H. Imergut, Polymer Handbook, 3rd Ed., New York (1989).
4. Cherdhirankorn T., W. Lerdwijitjarud, A. Sirivat, and R. G. Larson, "Dynamics of Vorticity Stretching and Breakup of Isolated Viscoelastic Droplets in an Immiscible Viscoelastic Matrix" *Rheologica Acta* **43**, 246-256 (2004).
5. De Bruijn, R. A., "Deformation and breakup of drops in simple shear flow", Ph.D.Thesis, Eindhoven University of Technology, 1989.

6. Elmendorp, J. J. and R. J. Maalcke, "A study on polymer blending microrheology: Part 1", *Polym Eng. Sci.* **25**, 1041-1047 (1985).

7. Flumerfelt, R. W."Drop breakup in simple shear fields of viscoelastic fluids", *Ind. Eng. Chem. Fundam.*, **11**, 312-318 (1972).

8. Grace, H. P., "Dispersion phenomena in high viscosity immiscible fluid systems and application of static mixers as dispersion devices in such systems", *Chem. Eng. Commun.* **14**, 225-277 (1982).

9. Guido, S., and M. Villone, "Three-dimensional shape of a drop under simple shear flow", *J. Rheol.* **42**, 395-415 (1998).

10. Hobbie, E. K. and K. B. Migler, "Vorticity elongation in polymeric emulsions," *Phys. Rev. Lett.* **82**, 5393-5396 (1999).

11. Lerdwijitjarud, W., R. G. Larson, and A. Sirivat, "Influence of weak elasticity of dispersed phase on droplet behavior in sheared polybutadiene/ Poly(dimethylsiloxane) blends," *J. Rheol.* **47**, 37-57 (2003).

12. Lerdwijitjarud, W., A. Sirivat, and R. G. Larson, "Influence of dispersed-phase elasticity on steady state deformation and breakup of droplets in simple shearing flow of immiscible polymer blends," *J. Rheol* **48**, 843-862 (2004).

13. Levitt, L., C. W. Macosko and S. D. Pearson, "Influence of normal stress difference on polymer drop deformation", *Polym. Eng. Sci.* **36**, 1647-1655 (1996).

14. Luciani, A., M. F. Champagne, L. A. Utracki, "Interfacial tension coefficient from the retraction of ellipsoidal drops", *J. Polym. Sci. Pol. Phys.* **35**, 1393-1403 (1997).

15. Mighri, F., A. Ajji, and P. J. Carreau, "Influence of elastic properties on drop deformation in elongational flow", *J. Rheol.* **41**, 1183-1201 (1997).

16. Mighri, F., P. J. Carreau, and A. Ajji, "Influence of elastic properties on drop deformation and breakup in shear flow" *J. Rheol.* **42**, 1477-1490 (1998).

17. Mighri, F. and M. A. Huneault, "Dispersion visualization of model fluids in a transparent Couette flow cell," *J. Rheol.* **45**, 783-797 (2001).

18. Migler, K. B., "Droplet vorticity alignment on model polymer blends," *J. Rheol.* **44**, 277-290 (2000).

19. Milliken, W. J., and L. G. Leal, "Deformation and breakup of viscoelastic drops in plannar extensional flows", *J. Non-Newtonian Fluid Mech.*, **40**, 355-379 (1991).

20. Rallison J. M., and A. Acrivos, "Numerical study of deformation and burst of a viscous drop in an extensional flow", *J. Fluid Mech.*, **89**, 191-200 (1978).

21. Tanpaiboonkul, P., W. Lerdwijitjarud, A. Sirivat, and R. G. Larson, "Transient and Steady State Deformations and Breakup of Dispersed –Phase Droplets of Immiscible Polymer Blends in Steady Shear Flow", *Submitted to Polymerl.*

22. Taylor, G. I., "The viscosity of a fluid containing small drops of another fluid", *Proc. R. Soc. London*, Ser. A **138**, 41-48 (1932).

23. Taylor, G. I., "The formation of emulsions in definable fields of flow", *Proc. R. Soc. London*, Ser. A **146**, 501-523 (1934).

24. Tretheway D. C., and L. G. Leal, "Deformation and relaxation of Newtonian drops in planar extensional flows of a Boger fluid" *J. Non-Newtonian Fluid Mech.* **99**, 81-108 (2001).

25. Varanasri, P. P., M. E. Ryan, and P. Stroeve, "Experimental study on the breakup of Model viscoelastic drops in uniform shear flow", *Ind. Eng. Chem. Res.* **33**, 1858-1866 (1994).

26. Jaenapn, V., Lerdwijitjarud, W., Sirivat A., "Oscillartory shear induced droplet deformation and breakup in immiscible polymer blends" Submitte to *J. Rheol. (2006)*.

27. Wannaborworn S., M. R. Mackley, and Y. Renardy, "Experimental observation and matching numerical simulation for the deformation and breakup of immiscible drops in oscillatory shear," *J. Rheol* **46**, 1279-1293 (2002).

28. Wu, S., "Formation of Dispered phase in incompatible polymer blends-interfacial and rheological effects." *Polym. Eng. Sci.* **27**, 335-343 (1987).

TABLES

Table I Polymers used

Polymers	Suppliers	M_w*	Specific gravity
HDPE1	Bangkok Polyethylene (Public) Limited (HDPE 1600J)	68,000	0.96
PS1	Aldrich Chemical Company, Inc.	162,000	1.04
PS2	Polyscience (Cat#18544)	50,000	1.05
PS3	Polyscience(Cat#23637)	800 – 5,000	1.05

* reported by the manufacturer

Table II Effect of viscosity ratio

Blend system	Blend components	T (°C)	Γ (mN/m)	G''_r	Wi_d	f (Hz)	τ_{rel} (sec)	τ_{osc} (sec)	Time scale ratio (τ_r)
A1	PS2/HDPE1	150	5.70	0.58	0.012 – 0.084	0.11	290	9.09	32
A2	PS2/HDPE1	155.5	5.61	0.12	0.0052 – 0.031	0.15	220	6.67	32
A3	PS2/HDPE1	158	5.54	0.06	0.0051 – 0.031	0.18	180	5.56	32

Table III Effect of time scale ratio ($\tau_r = \tau_{rel}/\tau_{osc}$)

Blend system	Blend components	T (°C)	Γ (mN/m)	G''_r	Wi_d	f (Hz)	τ_{rel} (sec)	τ_{osc} (sec)	Time scale ratio (τ_r)
A4	PS2/HDPE1	147	5.76	1.0	1.66 – 10.15	0.012	332	83.33	4
A4	PS2/HDPE1	147	5.76	1.0	1.71 – 10.30	0.05	332	20	16.6
A4	PS2/HDPE1	147	5.76	1.0	1.72 – 10.32	0.10	332	10	33.2
A4	PS2/HDPE1	147	5.76	1.0	1.89 – 11.35	0.192	332	5.2	63.8

Table IV Effect of droplet elasticity

Blend system	Blend Components	T (°C)	Γ (mN/m)	G''_r	Wi_d	f (Hz)	τ_{rel} (sec)	τ_{osc} (sec)	Time scale ratio (τ_r)
B1	PS3/HDPE1	148	5.76	0.12	0.0014 – 0.008	0.048	670	20.94	32
A2	PS2/HDPE1	155.5	5.61	0.12	0.0052 – 0.031	0.15	220	6.67	32
C1	PS1/HDPE1	232	4.89	0.12	0.378 – 2.26	0.33	105	3.03	32

FIGURE CAPTIONS

Figure 1 Schematic drawing of a single drop observed from the "side" and "top" views by optical microscopy, a and b: the long and short axes of the droplet in the flow-gradient plane, a^* : the a axis projected into the flow direction and c: the principal axis in the radial direction.

Figure 2 G' vs. frequency at different temperatures: (a) dispersed phases (PS1, PS2, PS3) using strain = 80% at frequency 0.1-1 rad/s, and strain = 10 % at frequency 1-100 rad/s; (b) matrix phases (HDPE1) using strain = 50% at frequency 0.1-1 rad/s, and strain = 10 % at frequency 1-100 rad/s.

Figure 3 G" vs. frequency at different temperatures: (a) dispersed phases (PS1, PS2, PS3) using strain = 80% at frequency 0.1-1 rad/s, and strain = 10 % at frequency 1-100 rad/s; (b) matrix phases (HDPE1 1600J) using strain = 50% at frequency 0.1-1 rad/s, and strain = 10 % at frequency 1-100 rad/s.

Figure 4 (a) G', at different temperatures, (b) G", at different temperatures.

Figure 5 Droplet deformation under shear at strain = 60 %, frequency = 0.18 Hz, G''_r = 0.06, Wi = 4.17 x 10^{-3}, τ_r = 32, T = 158 °C, d_o ~ 180 μm and gap 2,000 μm, at magnification 40X at various times in one cycle.

Figure 6 Deformation parameters vs. time of system C1 at strain 60%, frequency 0.33 Hz, τ_r = 32, G''_r ≈ 0.12, d_o ≈ 170 μm - 195 μm, gap = 2,000 μm: a) a* vs. time; b) c vs. time and c) Def* vs. time.

Figure 7 Amplitudes of the deformation parameters vs. Ca_m of system A1, A2, and A3 at τ_r= 32, d_o ≈ 190 μm - 205 μm, gap = 2,000 μm : T = 150 °C, G''_r = 0.58, G'_r = 0.032; T = 155.5 °C, G''_r = 0.12, G'_r = 0.009; T = 158 °C, G''_r = 0.06, G'_r = 0.0046: distance of drop from the center of plate ~ 6.8 mm: a) δa* vs. Ca_m; b) δc vs. Ca_m; c) δDef* vs. Ca_m.

Figure 8 Amplitudes of deformation parameters vs. Ca_m of system A4 at T = 147 °C, d_o = 185 μm - 200 μm, gap = 2,000 μm: frequency = 0.012 Hz, G''_r = 1, Re_{osc} = 1.45 x 10^{-11}; frequency = 0.05 Hz, G''_r = 1, Re_{osc} = 9.64 x 10^{-11}; frequency = 0.10 Hz, G''_r = 1, Re_{osc} = 2.37 x 10^{-10}; frequency = 0.192 Hz, G''_r = 1, Re_{osc} = 5.91 x 10^{-10}: distance of drop from the center of plate ~ 6.8 mm : a) δa* vs. Ca_m; b) δc vs. Ca_m, and c) δDef* vs. Ca_m.

Figure 9 Amplitudes of deformation parameters vs. Ca_m of system A2, B1, and C1 at $G''_r = 0.12$, $\tau_r = 32$, $d_o \approx 170\ \mu m$ - $190\ \mu m$, gap = 2000 μm: of PS3/HDPE1, T = 148°C, frequency = 0.048 Hz; PS2/HDPE1, T = 155.5 °C, frequency = 0.15 Hz and PS1/HDPE1, 232°C, frequency = 0.33 Hz: a) δa^* vs. Ca_m; b) δc vs. Ca_m; c) δDef^* vs. Ca_m.

Figure 10 Droplet breakup under oscillatory shear of system A1 where $Ca_c = 102.13$, $Wi_d = 2.48 \times 10^{-3}$, strain = 178, frequency = 0.2 Hz, $G''_r = 0.58$, $G'_r = 0.03$, time scale ratio = 58, T = 150 °C, $d_o = 167\ \mu m$, gap = 2000 μm, and magnification 40x.

Figure 11 Droplet breakup under oscillatory shear of system A3 where $Ca_c = 92.93$, $Wi_d = 2.6 \times 10^{-3}$, strain = 160, frequency = 0.2 Hz, $G''_r = 0.06$, $G'_r = 0.0045$, time scale ratio = 36, T = 158 °C, $d_o = 173\ \mu m$, gap = 2000 μm, and magnification 40x.

Figure 12 Critical capillary number vs. τ_r of: a) system A1 at T = 150 °C, $G''_r = 0.58$, $d_o \approx 165\ \mu m$ - $175\ \mu m$; b) system A3 T = 158°C, $G''_r = 0.06$, $d_o = 170\ \mu m$, gap = 2,000 μm.

Figure 13 Critical Weisenberg number (Wi_c) vs. τ_r of : a) system A1 at T = 150 °C, $G''_r = 0.58$, $d_o \approx 165\ \mu m$ - $175\ \mu m$; b) system A3 T = 158°C, $G''_r = 0.06$, $d_o = 165\ \mu m$ - $175\ \mu m$, gap = 2,000 μm.

Figure 14 Number of cycles required for drop breakup vs. τ_r of : a) system A1 at T = 150 °C, $G''_r = 0.58$, $d_o \approx 165\ \mu m - 175\ \mu m$; b) system A3 T = 158°C, $G''_r = 0.06$, d_o = 165 μm - 175 μm, gap = 2,000 μm.

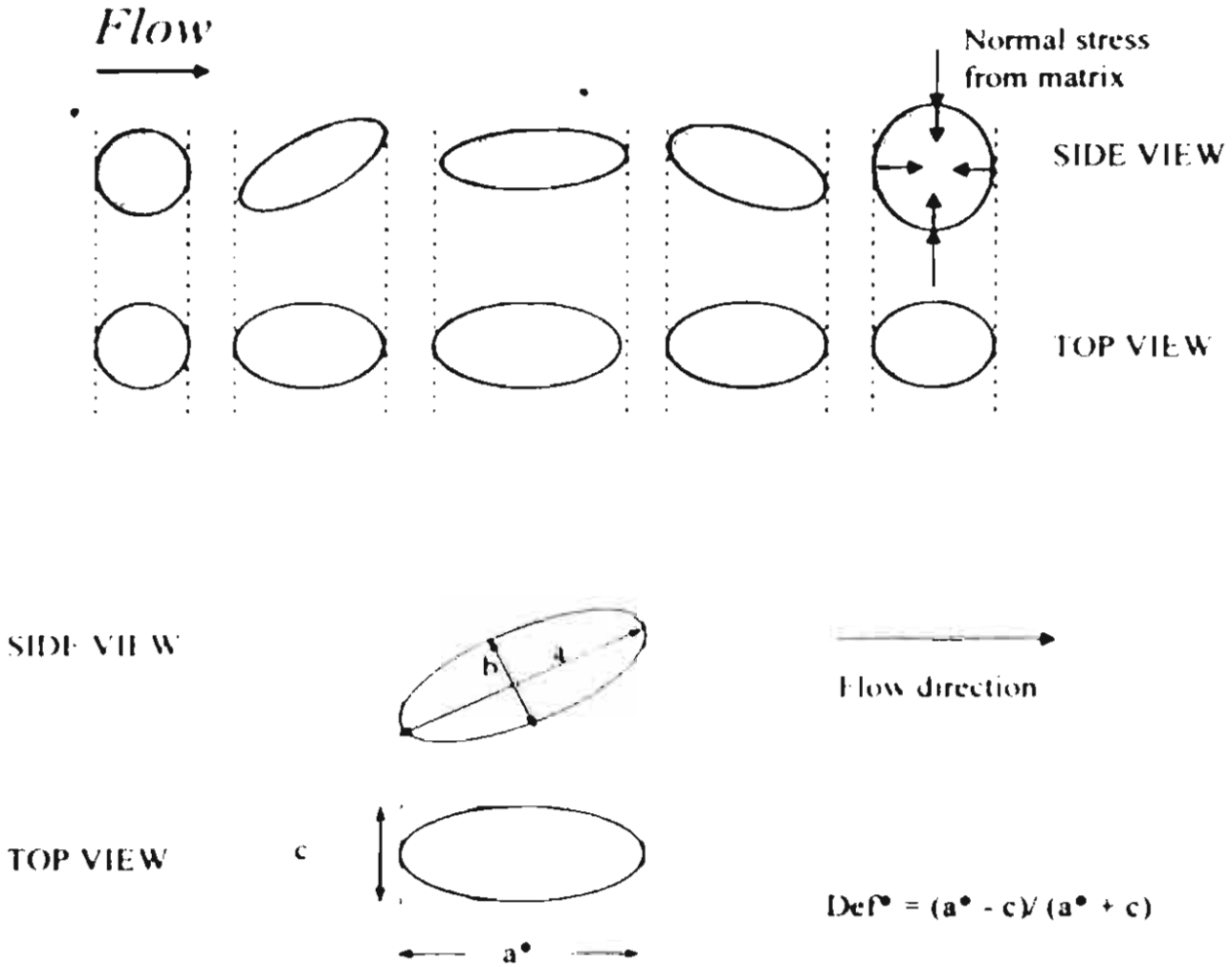

Figure 1 Schematic drawing of a single drop observed from the "side" and "top" views by optical microscopy, a and b: the long and short axes of the droplet in the flow-gradient plane, $a^{\bullet}$: the a axis projected into the flow direction and c: the principal axis in the radial direction.

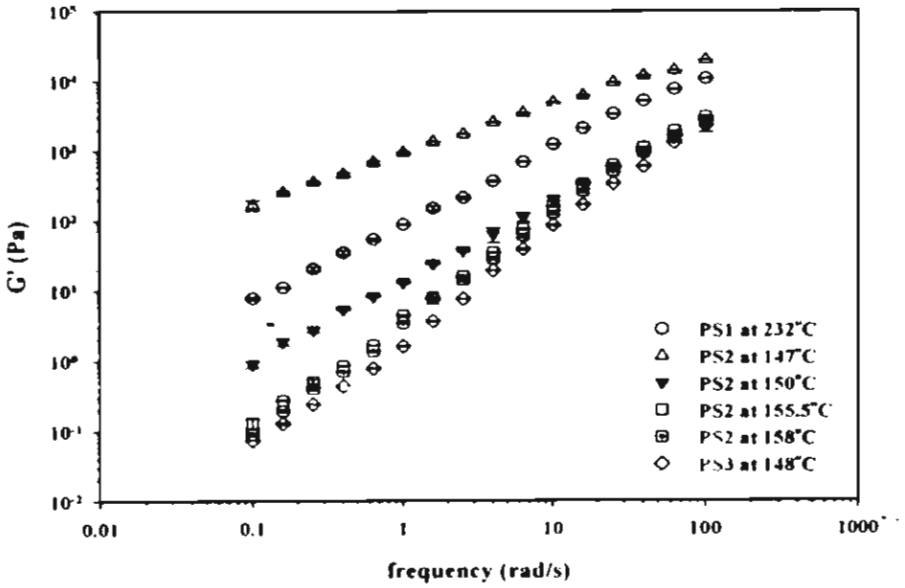

(a)

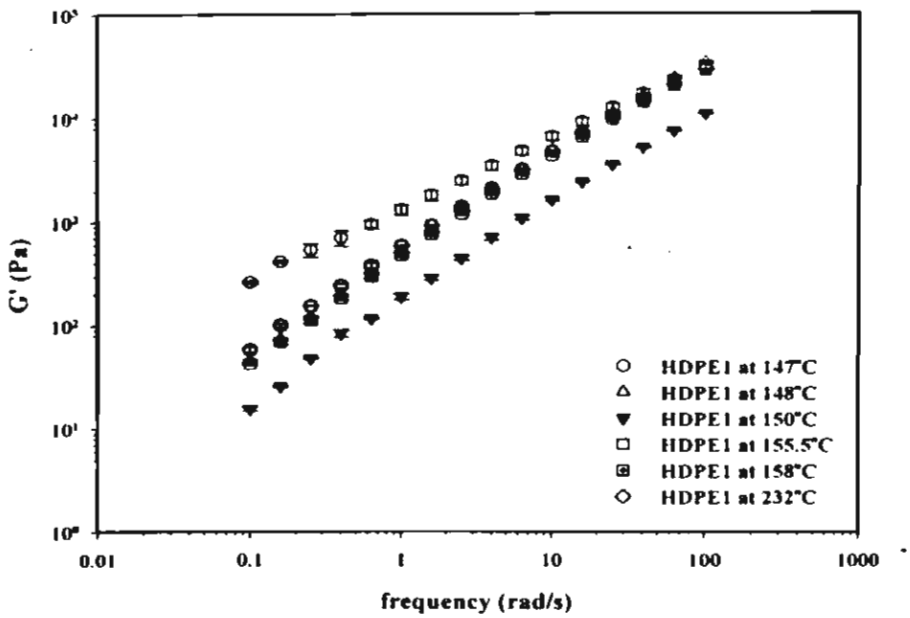

(b)

Figure 2 G' vs. frequency at different temperatures: (a) dispersed phases (PS1, PS2, PS3) using strain = 80% at frequency 0.1-1 rad/s, and strain = 10 % at frequency 1-100 rad/s; (b) matrix phases (HDPE1 1600J) using strain = 50% at frequency 0.1-1 rad/s, and strain = 10 % at frequency 1-100 rad/s.

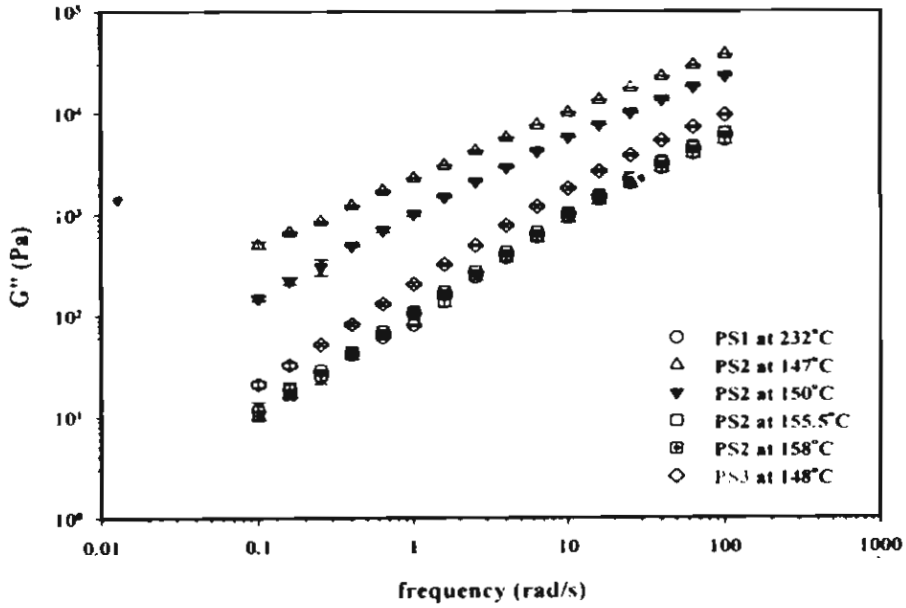

(a)

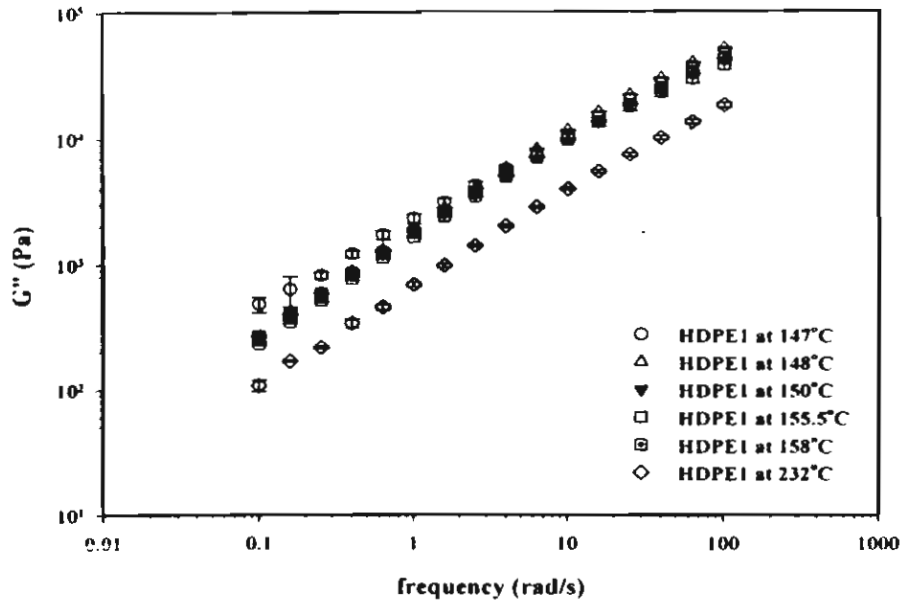

(b)

Figure 3 G" vs. frequency at different temperatures:
(a) dispersed phases (PS1, PS2, PS3) using strain = 80% at frequency 0.1-1 rad/s, and strain = 10 % at frequency 1-100 rad/s; (b) matrix phases (HDPE1 1600J) using strain = 50% at frequency 0.1-1 rad/s, and strain = 10 % at frequency 1-100 rad/s.

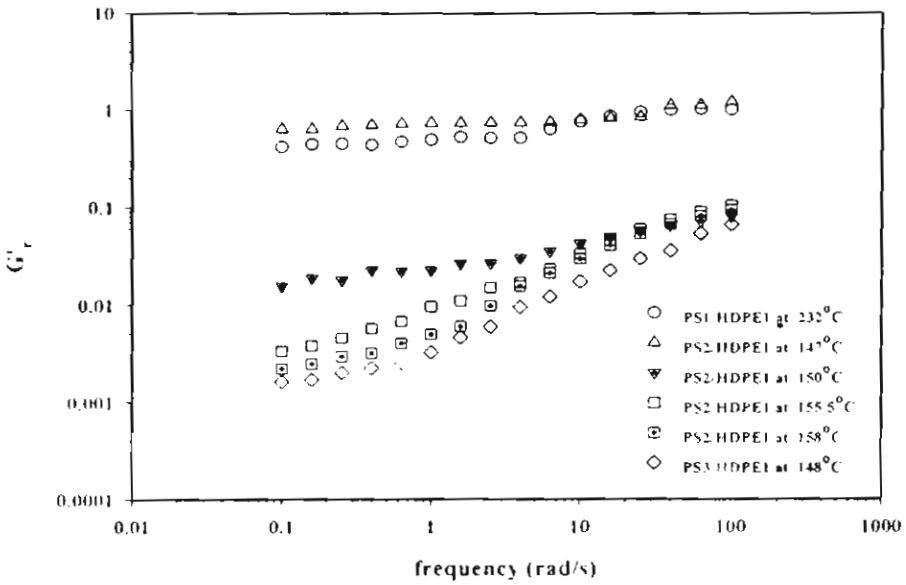

(a)

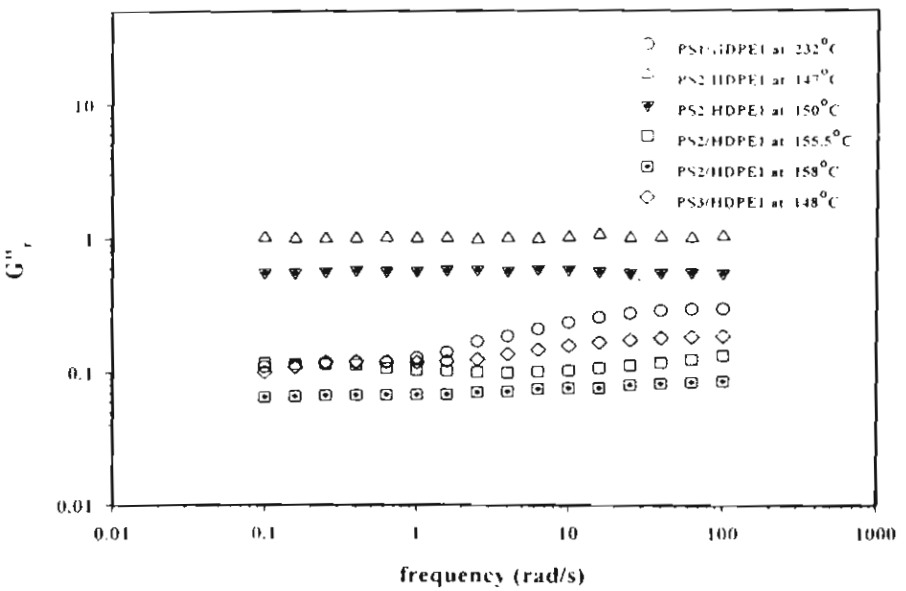

(b)

Figure 4 (a) G'_r at different temperatures, (b) G''_r at different temperatures.

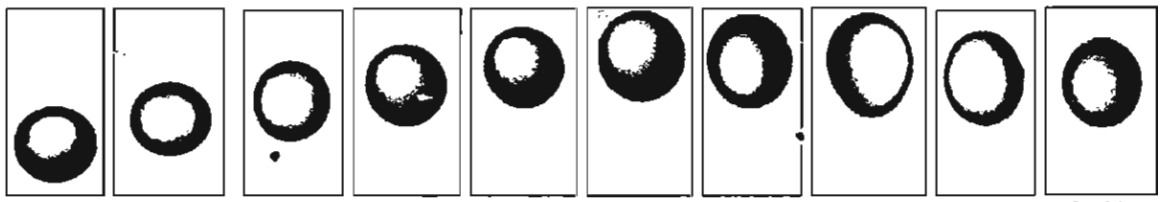

t (sec)	0	0.278	0.556	0.834	1.17	1.44	1.72	2.00	2.34	2.61
t/τ_{osc}	0	0.05	0.10	0.15	0.21	0.26	0.31	0.36	0.42	0.47

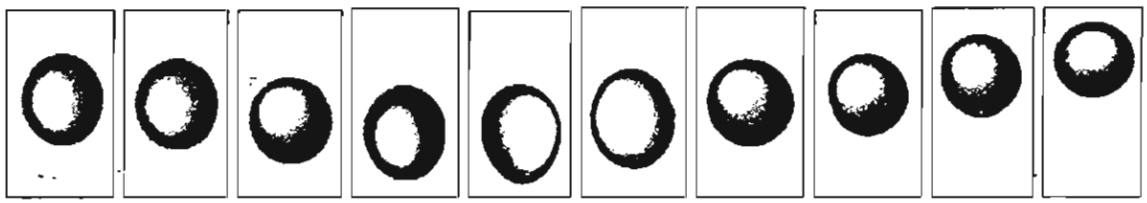

t (sec)	2.84	3.17	3.39	3.614	3.95	4.17	4.50	4.76	5.282	5.56
t/τ_{osc}	0.51	0.57	0.61	0.65	0.71	0.75	0.81	0.85	0.95	1.00

Figure 5 Droplet deformation of system A3 under shear at strain = 60 %, frequency = 0.18 Hz, $G''_r = 0.06$, Wi = 4.17×10^{-3}, $\tau_r = 32$, T = 158 °C, $d_o \sim 180$ μm and gap 2,000 μm, at magnification 40X at various times in one cycle.

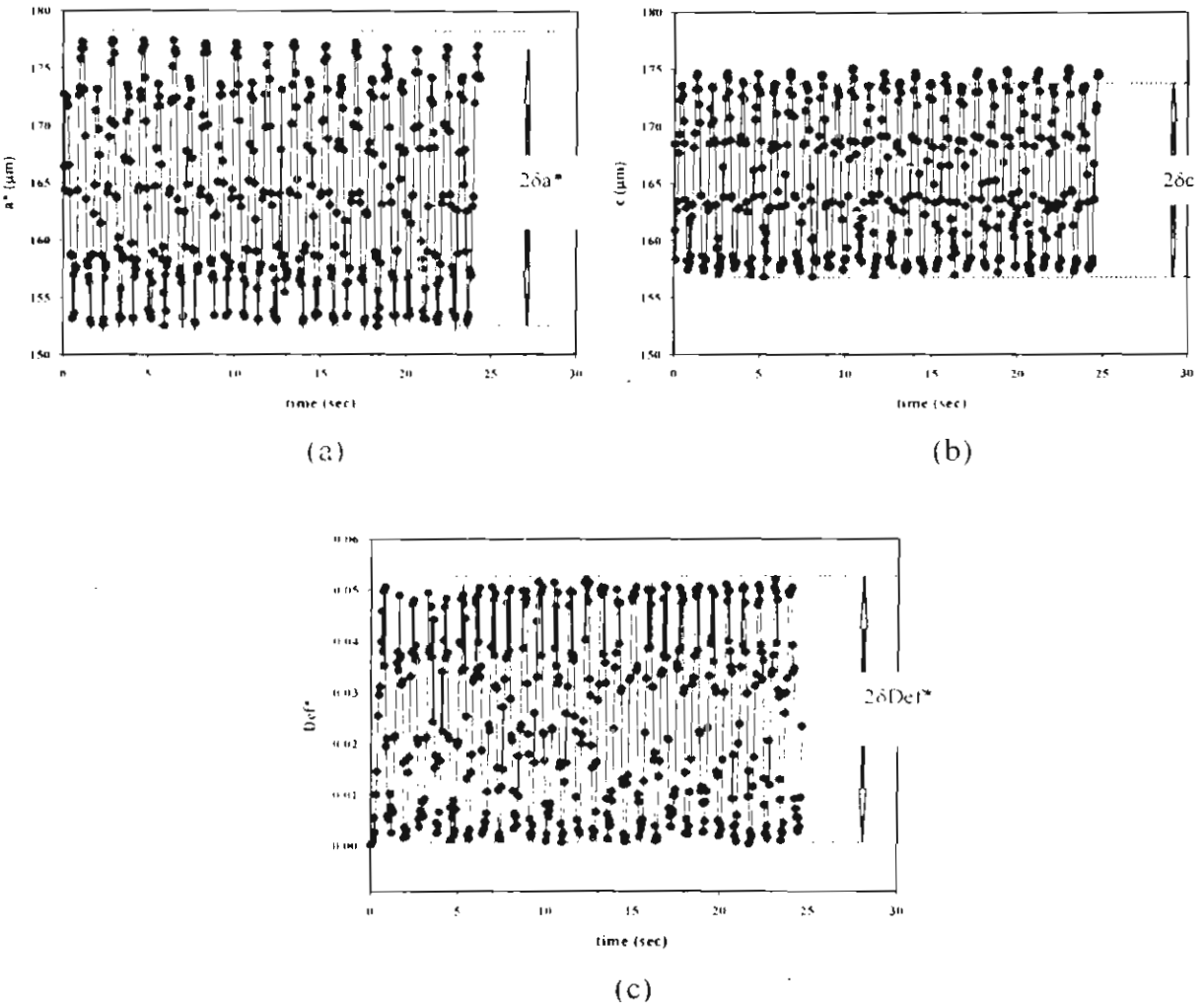

Figure 6 Deformation parameters vs. time of system C1 at strain 60%, frequency 0.33 Hz, $\tau_r = 32$, $G''_r = 0.12$, $d_o \approx 170\ \mu m$ - $195\ \mu m$, gap = 2,000 μm: a) a* vs. time; b) c vs. time; and c) Def* vs. time.

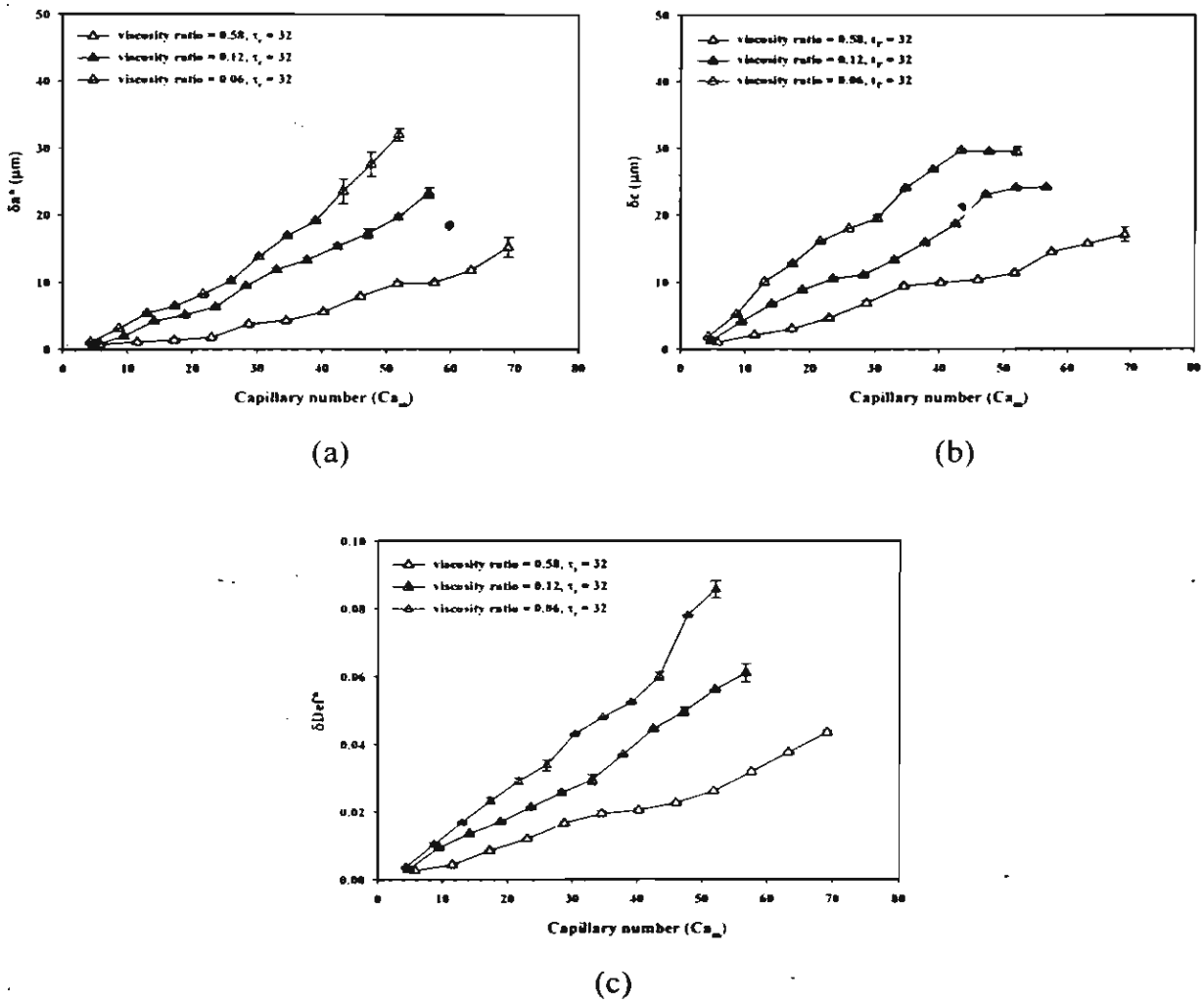

Figure 7 Amplitudes of the deformation parameters vs. Ca_m of systems A1, A2, and A3 at τ_r= 32, $d_o \approx$ 190 μm - 205 μm, gap = 2,000 μm: T = 150 °C, G" $_r$ = 0.58, G'$_r$ = 0.032; T = 155.5 °C, G" $_r$ = 0.12, G'$_r$ = 0.009; T = 158 °C, G" $_r$ = 0.06, G'$_r$ = 0.0046: distance of drop from the center of plate ~ 6.8 mm: a) δa* vs. Ca_m; b) δc vs. Ca_m; c) δDef* vs. Ca_m.

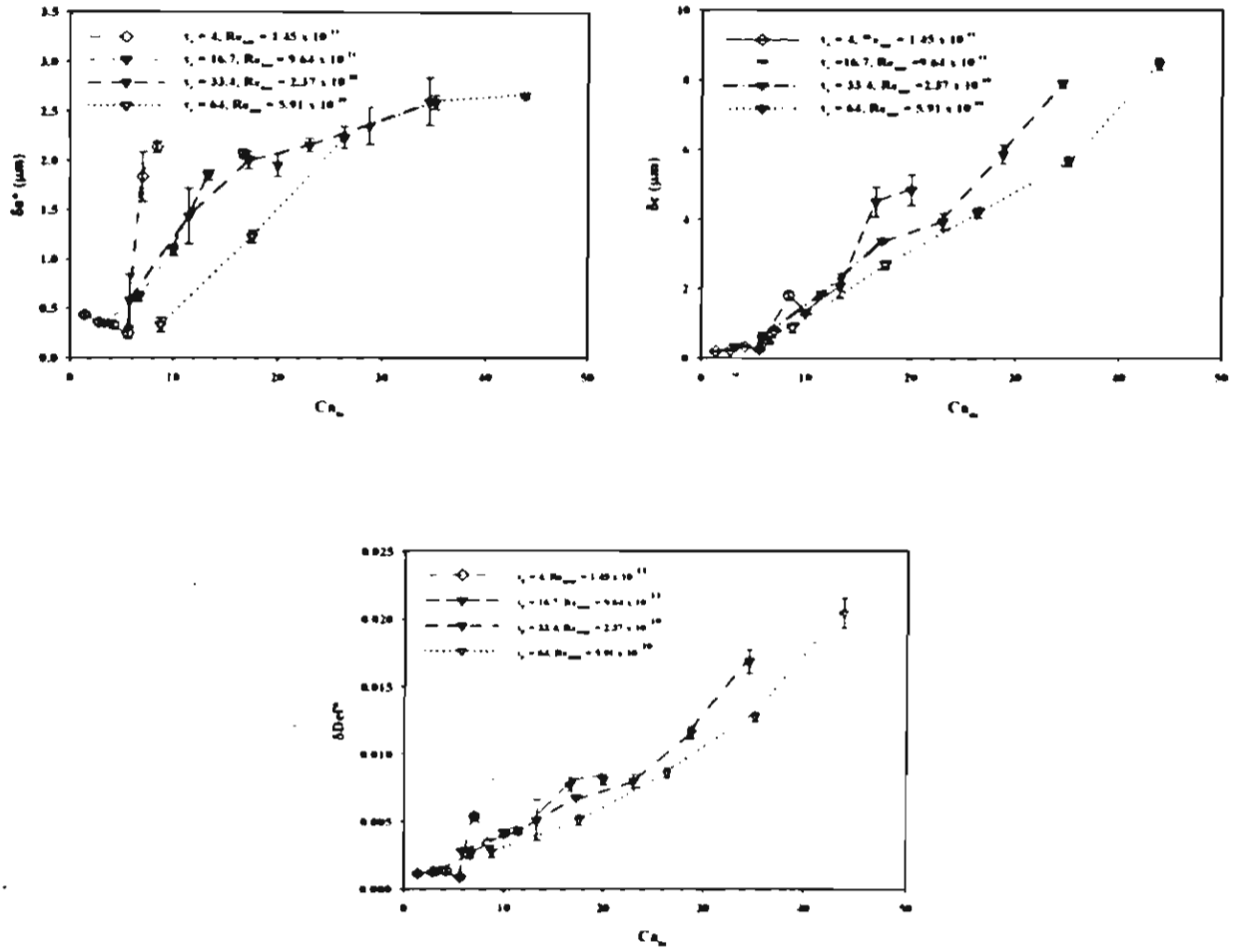

Figure 8 Amplitudes of deformation parameters vs. Ca_m of system A4 at T = 147 °C, d_o = 185 μm - 200 μm, gap = 2,000 μm: frequency = 0.012 Hz, G"$_r$ = 1, Re_{osc} = 1.45 x 10^{-11}; frequency = 0.05 Hz, G"$_r$ = 1, Re_{osc} = 9.64 x 10^{-11}; frequency = 0.10 Hz, G"$_r$ = 1, Re_{osc} = 2.37 x 10^{-10}; frequency = 0.192 Hz, G"$_r$ = 1, Re_{osc} = 5.91 x 10^{-10}; distance of drop from the center of plate ~ 6.8 mm: a) δa* vs. Ca_m; b) δc vs. Ca_m; and c) δDef* vs. Ca_m.

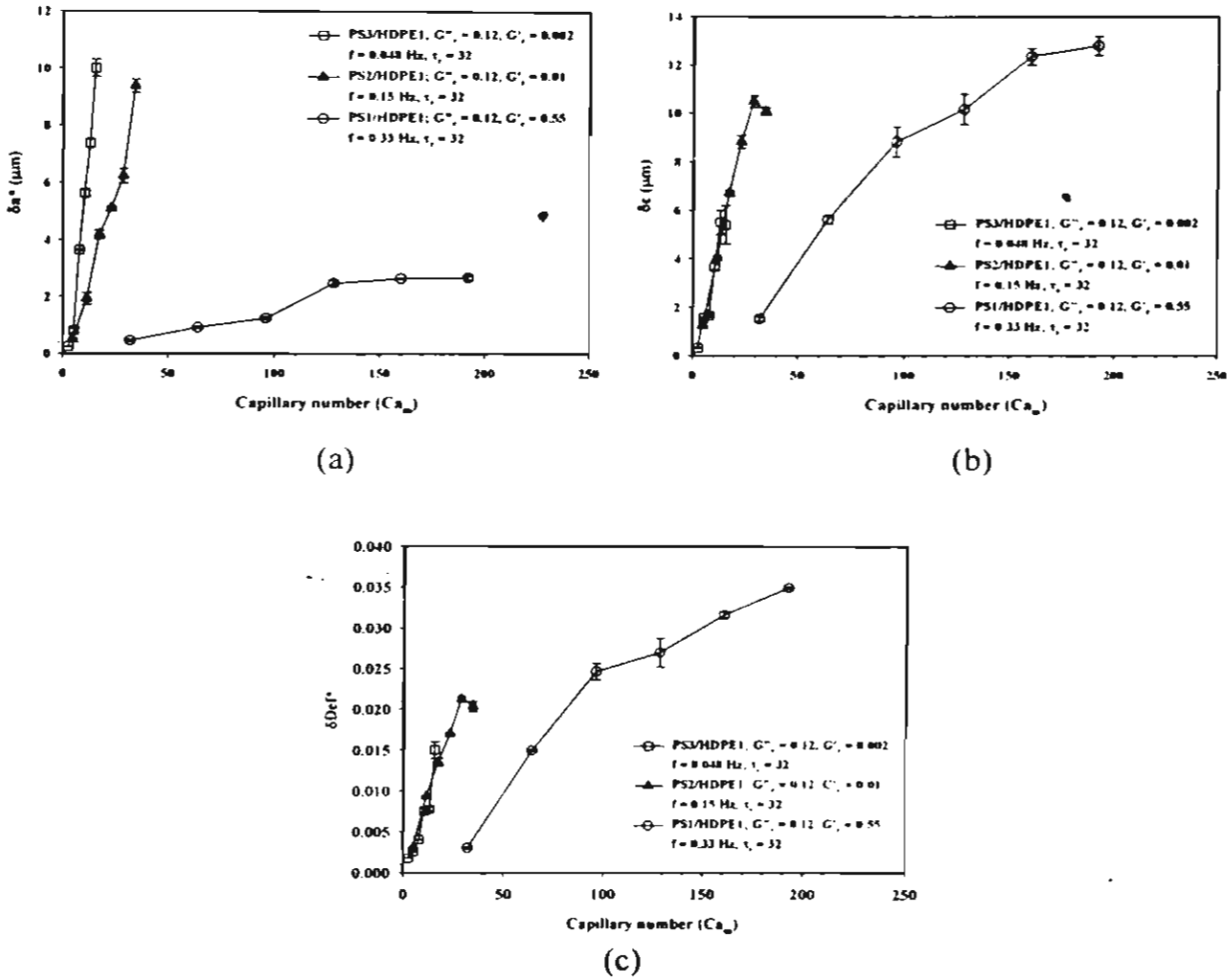

Figure 9 Amplitudes of deformation parameters vs. Ca_m of systems A2, B1, and C1 at $G''_r = 0.12$, $\tau_r = 32$, $d_o \approx 170\ \mu m$ - $190\ \mu m$, gap = 2000 μm: system B1, T = 148°C, frequency = 0.048 Hz; system A2, T = 155.5 °C, frequency = 0.15 Hz; and system C1, T = 232°C, frequency = 0.33 Hz. a) δa^* vs. Ca_m; b) δc vs. Ca_m; c) δDef^* vs. Ca_m.

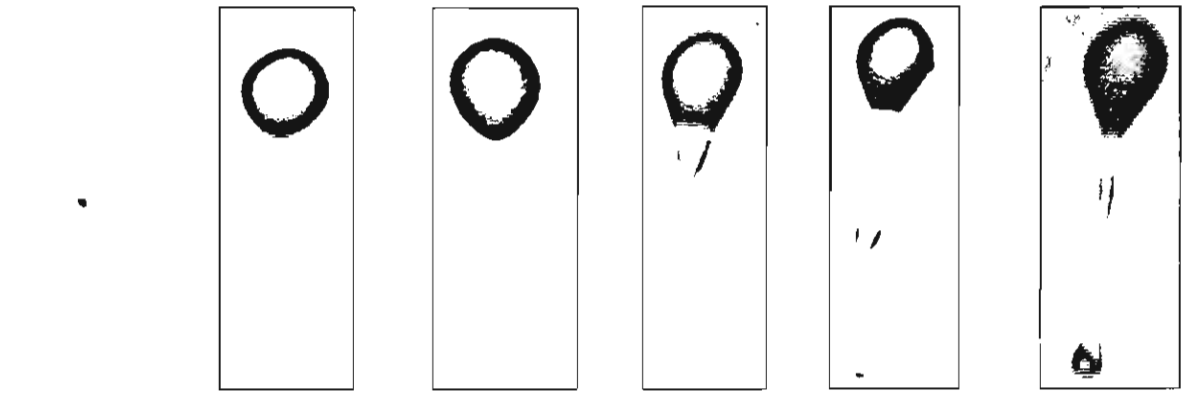

t (sec)	10	60	371	684	874
t/τ_r	2	12	74	136	174

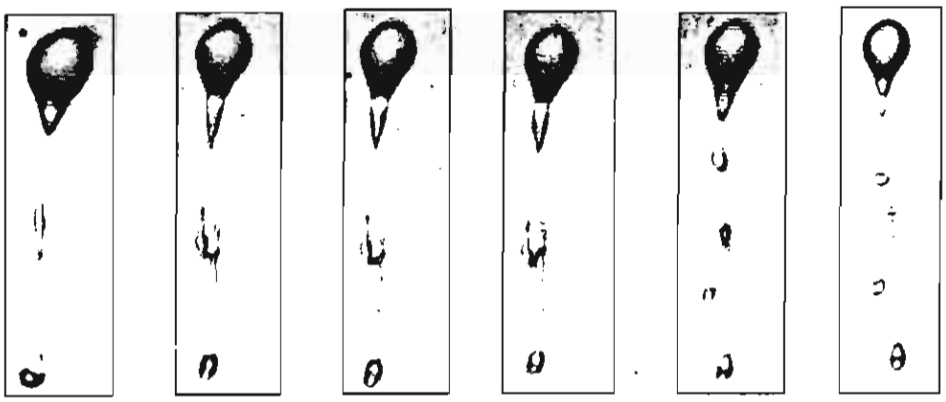

t (sec)	956	1014	1035	1050	1065	1140
t/τ_r	191	202	207	210	213	228

Figure 10 Droplet breakup under oscillatory shear of system A1 where Ca_c = 102.13, $Wi_d = 2.48 \times 10^{-3}$, strain = 178, frequency = 0.2 Hz, G''_r = 0.58, G'_r = 0.03, time scale ratio = 58, T = 150 °C, d_o = 167 μm, gap = 2000 μm, and magnification 40x.

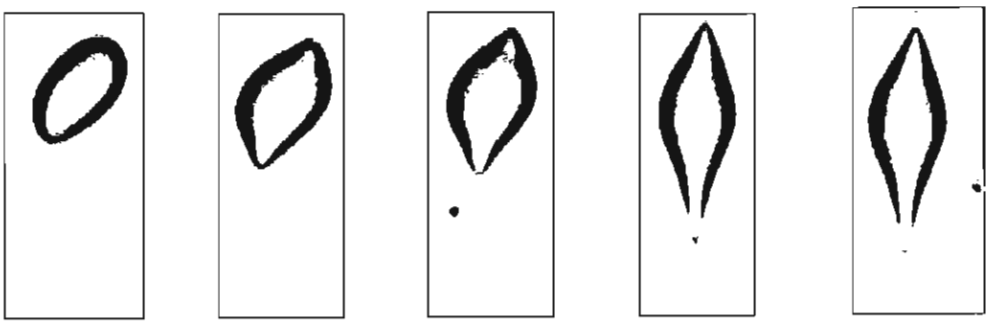

t (sec)	40	81	104	132	160
t/τ_r	8	16	20	26	32

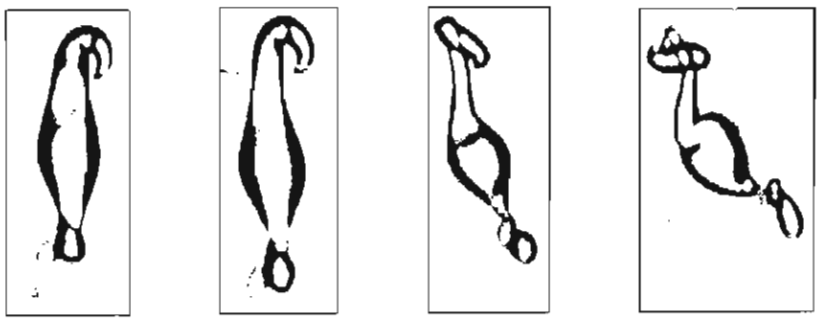

t (sec)	250	305	395	485
t/τ_r	50	61	79	97

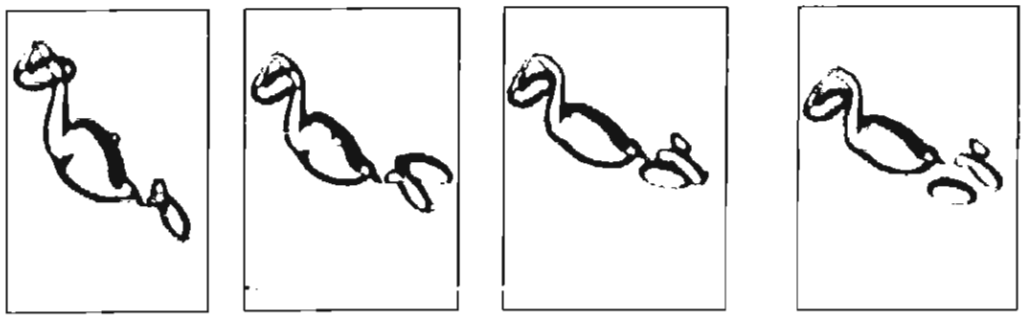

t(sec)	545	604	688	719
t/τ_r	109	120	137	143

Figure 11 Droplet breakup under oscillatory shear of system A3 where $Ca_c = 92.93$, $Wi_d = 2.6 \times 10^{-3}$, strain = 160, frequency = 0.2 Hz, $G''_r = 0.06$, $G'_r = 0.0045$, time scale ratio = 36, T = 158 °C, d_o = 173 μm, gap = 2000 μm, and magnification 40x.

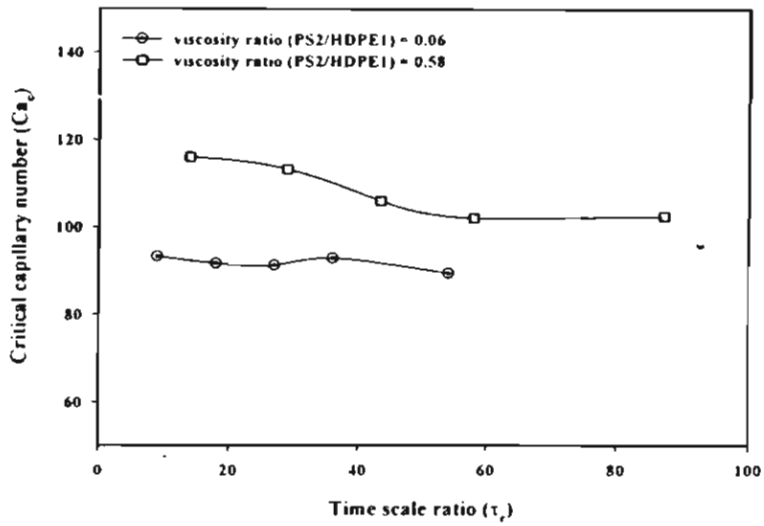

Figure 12 Critical capillary number vs. τ_r of: a) system A1 at T = 150 °C, $G''_r = 0.58$, $d_o \approx 165\ \mu m$ - 175 μm; b) system A3 T = 158°C, $G''_r = 0.06$, $d_o = 170\ \mu m$, gap = 2,000 μm.

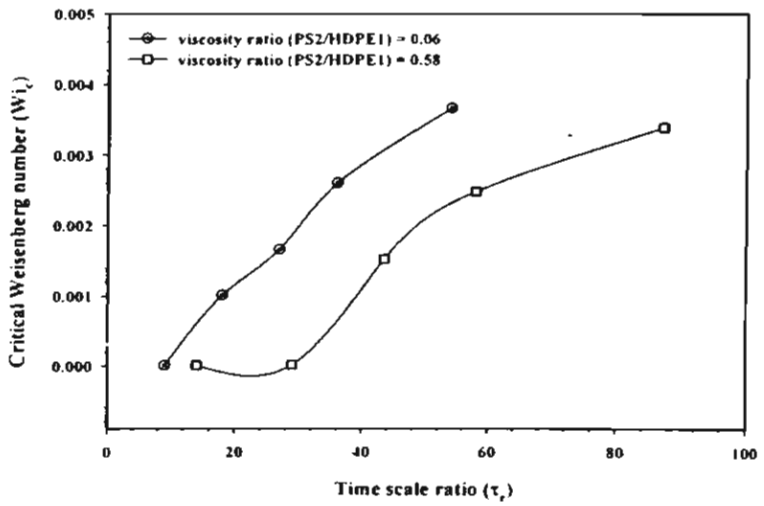

Figure 13 Critical Weisenberg number (Wi_c) vs. τ_r of: a) system A1 at T = 150 °C, $G''_r = 0.58$, $d_o \approx 165\ \mu m$ - 175 μm; b) system A3 T = 158°C, $G''_r = 0.06$, $d_o = 165\ \mu m$ - 175 μm, gap = 2,000 μm.

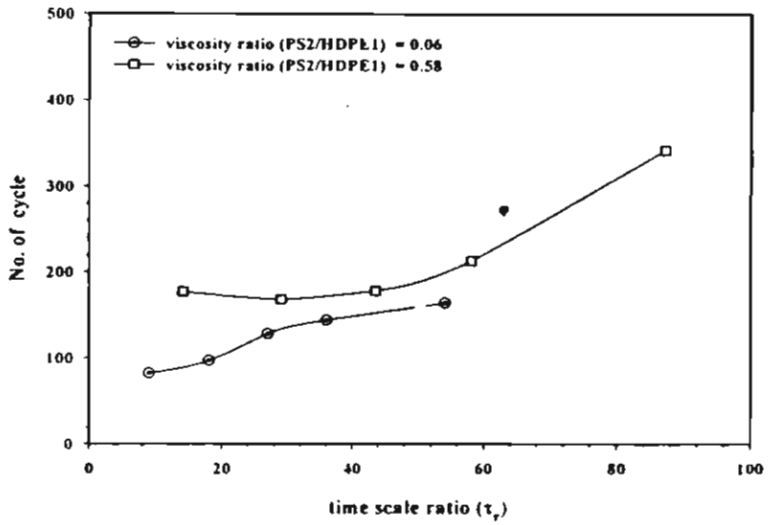

Figure 14 Number of cycles required for drop breakup vs. τ_r of: a) system A1 at T = 150 °C, $G''_r = 0.58$, $d_o \approx 165\ \mu m$ - $175\ \mu m$; b) system A3 T = 158°C, $G''_r = 0.06$, d_o = 165 μm - 175 μm, gap = 2,000 μm.

Chapter 3: Dynamics of Vorticity Stretching and Breakup of Isolated Viscoelastic Droplets in an Immiscible Viscoelastic Matrix

Thipphaya Cherdhirankorn[a], Wanchai Lerdwijitjarud[b], Anuvat Sirivat[a,#], and Ronald G. Larson[c]

[a] Petroleum and Petrochemical College, Chulalongkorn University, Bangkok 10330, Thailand

[b] Department of Materials Science and Engineering, Faculty of Engineering and Industrial Technology, Silpakorn University, Nakorn Pathom 73000, Thailand

[c] Department of Chemical Engineering, University of Michigan, Ann Arbor, Michigan 48109, USA

Keywords: Viscoelastic droplet, vorticity stretching, immiscible blends

Abstract

The effect of droplet elasticity on transient deformation of isolated droplets in immiscible polymer blends of equal viscosity was investigated. In terms of the deformation parameter, Def* = a^*- c/ a^*+ c where a^* and c are apparent drop principal axes, it undergoes two cycles of positive oscillations before reaching a negative value, followed by one cycle of oscillation before attaining a steady state negative value. This behavior was observed when Capillary number, *Ca*, was varied between 3 and 9 at a fixed Weissenber number, Wi, of 0.31, and when *Ca* number was held fixed at 8 and Wi number was varied between 0.21 and 0.40. In another blend of relatively lower Wi number of 0.21, one cycle of oscillation in Def* was observed before reaching steady state negative values when *Ca* number was varied between 3 and 14. The steady state Def* varies inversely with *Ca* number, with a stronger dependence for the blend with higher Wi number. The magnitude of oscillation increases with increasing *Ca* and Wi numbers. The critical *Ca* was found to be 12 and 14 for the two blends studied; these values are about 30 times greater than that of Newtonian blends.

Corresponding author Email: anuvat.s@chula.ac.th

INTRODUCTION

For Newtonian polymer blends in a simple shear flow, the morphology of the minor (or droplet) phase is governed mainly by two dimensionless parameters: the viscosity ratio, i.e., the ratio of droplet viscosity to matrix viscosity; and the capillary number, the ratio of viscous to interfacial forces (Taylor 1932,1934):

$$Ca = \frac{D_o \dot{\gamma} \eta_m}{2\Gamma} \tag{1}$$

where $\dot{\gamma}\eta_m$ is the viscous shear stress, with $\dot{\gamma}$ is the shear rate and η_m the matrix viscosity, D_o is initial droplet diameter, and Γ is the interfacial tension.

A steady applied shearing flow that is not so fast as to lead to droplet rupture will eventually stretch a droplet into a roughly ellipsoidal steady-state shape, and the steady-state degree of deformation, defined as the deformation parameter Def, is approximately linearly related to the capillary number as (Taylor 1932,1934)

$$Def \equiv \frac{a-b}{a+b} = Ca\,\frac{19\eta_r + 16}{16\eta_r + 16} \tag{2}$$

where a and b are the lengths of the major and minor axis of the deformed droplet, respectively. Taylor (1934) predicted that the critical point at which the viscous force overcomes the interfacial force leading to droplet breakup occurs at $Ca_c \approx 0.5$ and $Def_c \approx 0.5$ for a steady (or quasi-steady, if the flow rate is very slowly increased) simple shearing flow with a viscosity ratio of around unity. Here, the subscript "c" stands for the critical condition for breakup. These basic predictions have been confirmed and refined in a number of detailed single-droplet experiments (Rumscheid and Mason 1961; Grace 1982; Bentley and Leal 1986; Guido and Villone 1997). However, when the viscosity ratio is higher than four, no breakup can be observed (Grace 1982). These results show that for Newtonian fluids, droplet deformation and breakup is strongly influenced by viscosity ratio, a result that emphasizes the importance of controlling this parameter carefully in any attempt to study the effects of other factors, such as viscoelasticity, on droplet deformation and breakup.

The above results were obtained for Newtonian droplets and matrix fluids; however, most polymers are viscoelastic under normal processing conditions, and so elasticity of the droplet and matrix phases should be an important factor affecting the behavior of droplets under a flow field. It has long been noticed, for example, that in blends of viscoelastic polymer melts, the steady-state average droplet size that results from breakup and coalescence of droplets under shear corresponds to a much higher capillary number than is seen in blends of Newtonian liquids at comparable viscosity ratios. Wu (1987) observed, for example, that the steady-state droplet size in extruded viscoelastic polymer blends at a viscosity ratio of unity is around ten times higher than would be obtained for Newtonian components at the same viscosity and at the same shear rate. Lerdwijitjarud *et al.* (2002) found that in blends of 20% polystyrene in polyethylene sheared in a rheometer, the steady-state droplet size corresponded to a capillary number ranging from 2 to 30, depending on the relative magnitudes of the normal stress differences in the droplet and matrix phases and on the viscosity ratio. These capillary numbers are from 4 to 80 times higher than the critical capillary number for breakup of a Newtonian droplet in a Newtonian matrix. While it might be thought that this large increase in droplet size and hence capillary number could be due in part to coalescence effects present in blends, Lerdwijitjarud *et al.* (2003) showed recently that in a 20% blend of a Newtonian liquid in a Newtonian matrix the steady-state capillary number is actually lower than the critical capillary number for breakup of an isolated droplet; i.e., the disturbances to the flow produced by the presence of the other droplets enhances breakup of a given droplet to an extent that more than offsets any increase in droplet size due to coalescence. Thus, the high steady-state capillary numbers observed in blends of viscoelastic polymers must be attributed to the role of viscoelasticity.

Elasticity in the droplet or matrix phase can be quantified by the Weissenberg number Wi, a ratio of elastic to viscous forces, which we here will estimate using either the first normal stress difference N_1 or elastic modulus G' as a measure of the elastic forces and the shear stress as a measure of the viscous forces. Like the capillary number, the Weissenberg number increases with increasing shear rate, since elastic forces generally increase with shear rate more rapidly than do viscous forces. For a given droplet size, Wi and Ca are qualitatively proportional to

each other; however, since Ca depends on droplet diameter and Wi does not, these two dimensionless numbers can be varied independently by varying both the shear rate and the droplet size for a given pair of viscoelastic fluids. Since both phases can be elastic, there are two Weissenberg numbers, the droplet Weissenberg number Wi_d and the matrix Weissenberg number Wi_m. Since the elastic stresses in the droplet depend on the strength of the flow in the droplet, which is, in turn dependent on the viscosity ratio (more viscous droplets have weaker internal flows), it is clear that in general there is a coupling between the viscosity ratio and the strength of the elastic forces in the droplet. To minimize this influence, in what follows, we will work with fluids having viscosity ratios near unity, and use the macroscopic shear rate to characterize the flow inside the droplet. That is, following the work of Lerdwijitjarud *et al.* (2002), we will not attempt to use the actual flow in the droplet to estimate the droplet Weissenberg number, but will characterize the elasticity of the droplet using Wi_d defined by the droplet fluid properties at the macroscopic shear rate measured on the pure droplet fluid in a rheometer.

Recently, single viscoelastic droplets in Newtonian or viscoelastic matrices have been observed microscopically in simple shearing flows. Lerdwijitjarud *et al.* (2003) observed deformation and breakup of isolated droplets of weakly elastic fluid ($Wi_d \leq 0.02$) in a Newtonian matrix, and found that droplet elasticity produces a slight (up to around 20%) increase in Ca_c, the critical capillary number for droplet breakup. The breakup mechanism appeared to be similar to that in a Newtonian fluid; i.e., the droplet deformed increasingly in the flow direction as the shear rate was gradually increased, until breakup occurred. Elasticity of the droplet produced a reduction in the degree of deformation at any given shear rate and a greater critical deformation at breakup, resulting in a higher Ca_c. However, at the highest Weissenberg number, this effect appeared to be saturating, leading to only a modest increase in Ca_c.

Mighri *et al.* (1998) investigated the influence of elastic properties on droplet deformation and on the critical shear rate, or critical capillary number Ca_c for breakup. The deformed elastic droplet was roughly spheroidal with slightly sharpened edges while a Newtonian droplet retained smooth curved ends. Mighri *et al.* (1998) reported that the degree of droplet deformation, the critical shear rate for breakup, and the breakup time after startup of shearing increased with increasing

elasticity ratio between the droplet and the matrix fluids. They defined the elasticity ratio, k', as the ratio of the Maxwell relaxation time (λ) of the droplet phase to that of the matrix phase, where $\lambda = N_{1i}/2\eta\dot{\gamma}^2$, where N_{1i} is the first normal stress difference. Breakup occurred by an unsteady deformation of the droplet into a thin and long thread, followed by end pinching, and undulations along the droplet surface, finally resulting in a series of alternating large and small (or "satellite") droplets. Moreover, they found that for a low or modest elasticity ratio, $k' \leq 4$, the critical capillary number Ca_c for droplet breakup in steady shearing flow increased with increasing k', reaching $Ca_c \approx 1.75$ at high elasticity ratio, $k' \approx 4$, compared to $Ca_c \approx 0.5$ for Newtonian droplets. Thus, droplet resistance to deformation and breakup increases with increasing elasticity ratio of droplet to matrix phase. While the elasticities of the droplets studied by Mighri *et al.* (1998) were higher than those studied by Lerwijitjarud *et al.* (2003), the droplets in both studies deformed in the flow direction, and the increase in critical capillary number produced by elasticity saturated at a relatively modest values near unity, far below the steady-state values observed in highly viscoelastic polymer blends. These studies, and those described below, suggest that large increases in Ca_c result from a new mode of droplet deformation and breakup for highly elastic droplets.

A new, viscoelastic, mode of droplet deformation, that of droplet extension *in the vorticity direction* (perpendicular to both the shear and shear gradient directions) was apparently first reported for an elastic polymer droplet in a polymer matrix by Bartram *et al.* (1975). An apparently related phenomenon of *widening* of an extended viscoelastic droplet in a highly viscoelastic matrix was later observed by Levitt and Macosko (1996), who suggested that there is a relationship between the second normal stress difference of droplet and matrix phase and the degree of widening. Hobbie and Migler (1999) studied dilute emulsions of viscoelastic droplets in viscoelastic matrices at high shear rate and also observed elongation of the droplet in the vorticity direction at $\dot{\gamma} \sim 280\ s^{-1}$ for viscosity ratio $\eta_r = 1.8$. By extrapolating data at high shear rates to lower rates, they obtained critical capillary numbers for droplet vorticity alignment of around 53, 13, and 11 for viscosity ratios, η_r, of 1.8, 22, and 240, respectively. The increase in critical capillary number for vorticity

alignment with viscosity ratio is consistent with a mechanism involving droplet elasticity, since a higher droplet viscosity would require a higher external flow rate to attain the same internal flow rate within the droplet, which would be needed to maintain a high elasticity of the droplet fluid.

Migler (2000) observed the deformation of highly elastic droplets in a polymeric matrix under a shear flow. The viscosity ratio was near unity, but the elasticity ratio of the droplet to the matrix was higher than 100; that is, the matrix phase was nearly Newtonian under the conditions of the experiments. In a weak shear and for small droplets [Ca < 5], the droplet orientation was found to be along the flow direction, whereas in a strong shear and for large droplets [Ca > 5], the orientation was along the vorticity axis with a broad distribution of aspect ratios.

Mighri and Huneault (2001) studied the deformation and breakup of a single droplet of viscoelastic Boger fluid in a Newtonian matrix, sheared in a transparent Couette flow cell. At low shear rate, they found that the steady-state deformation increased with shear rate as expected, but above a critical shear rate [Ca ~ 5] the deformed drop began contracting in the flow direction and changed its orientation to the vorticity axis. With further increases in shear rate, this elongation in the vorticity direction increased until breakup finally occurred at a capillary number no higher than Ca~35. They proposed that the critical shear stress for reorientation of the droplet in the vorticity direction was probably related to the values of the first and second normal stress differences and their dependencies on shear rate. They also suggested that this reorientation occurred because of a the flow-induced circulatory flow in the droplet that produced an elastic circular hoop stress in the plane containing the shear and the shear gradient directions that squeezed fluid out along the axis perpendicular to this plane, that is, along the vorticity axis (Hobbie and Migler 1999; Migler 2000). They surmised that in a startup of a steady shearing flow, the deforming viscous stress rapidly reached steady state, but the normal stresses generated by the dispersed phase required a longer time, which caused a gradual increase in droplet elongation along vorticity axis until either a steady-state deformation was reached or breakup occurred. When a droplet was highly stretched in the vorticity direction, they observed small rocking instabilities in the velocity gradient direction causing the two ends of the droplet to sample significantly

different velocities periodically, which ultimately tore apart the droplet into two or more smaller drops.

In our work reported below, we take a further step towards understanding the behavior of commercial blends by using elastic polymer melts for both the droplet phase and the matrix phase. To neutralize any effect of variations in the viscosity ratio, we choose pairs of commercial polymers whose viscosity ratios remain relatively constant near unity when shear rate is varied. Using a flow cell mounted on an optical microscope, we observe the transient deformations of isolated droplets after startup of steady shear flow between parallel disks. By varying droplet size and shear rate, the effects of capillary number and elasticity (or droplet Weissenberg number) are isolated and investigated at fixed viscosity ratio very near unity. Our findings confirm those of Mighri and Huneault, who used nearly Newtonian matrix fluids, but, in addition, we find that when both the droplet fluid and the matrix fluid are highly elastic, droplet deformations during start-up of steady shearing show large oscillations before reaching steady state.

EXPERIMENTS

A. Materials

High density polyethylene and polystyrene (suppliers and grades given in Table 1) were used as matrix and droplet phases, respectively. Both polystyrene grades were obtained from the manufacturers in the form of flake; they were crushed and size-selected by passing the flakes through a 425-mm sieve. To eliminate volatile components, all polymers were heated to around 80°C under vacuum for 12 hours. The polymer blend systems and their experimental temperatures are listed in Table 2.

B. Rheological Characterization

Each polymer was molded into a disk, 25 mm in diameter and 1 mm thick by using a compression mold (Wabash, model V50H-18-CX) at 145°C for HDPE1 and PS1, and at 135°C for HDPE2 and PS2 under a force of 10 tons. We used a cone-and-plate rheometer (Rheometrics Scientific: Model ARES, 25-mm plate diameter with cone angle 0.1 rad) to obtain viscosities and first normal stress differences of the pure polymers. From the rheological properties of pure polymers at various temperatures, the desired pairs of polymers and operating temperatures were selected for further study; and their steady-state viscosities and first normal stress differences as functions of shear rate are shown in Fig. 1 (a) and (b). At low shear rates, the ratio of droplet-to-matrix first normal stress differences N_{1r} of system B could not be precisely determined due to the force-measurement limitations of the rheometer. However, in the low-shear-rate and low-frequency regimes, $N_1(\dot{\gamma})$ is approximately equal to twice G' (ω) at $\dot{\gamma}=\omega$, thus N_{1r} can be estimated by the corresponding ratio of storage moduli, G'_r. The Weissenberg number (Wi) of both matrix and dispersed phases at testing conditions is also given in Table 3. The viscosity ratios and G' ratios of the two polymer systems are shown in Fig. 2. In addition, the stabilities of all polymers to thermal degradation were tested at their experimental temperatures by measuring the viscosity at a constant shear rate, 0.5 s^{-1}, for 4 hours; in all cases the viscosity values remain unchanged, allowing us to conduct blend experiments on each system for periods as long as four hours.

C. Observations of an Isolated Droplet in Shearing Flow

1. Shearing Apparatus

To observe the droplet behaviors in simple shearing flow, we used a flow cell (Linkam CSS 450, Linkam Scientific Instruments Ltd., UK) consisting of two transparent quartz parallel disks mounted on an optical microscope (Leica DMRPX, Leica Imaging Systems LTd., Cambridge, England), and connected to a CCD camera (Cohu 4910, Cohu Inc., CA). In addition, the images were analyzed on a computer using the Scion image software.

2. Sample Preparation

HDPE used as the matrix polymer was molded into a disk 25 mm in diameter and 0.5-1 mm thick by compression molding at 145°C for HDPE1 and 135°C for HDPE2. Various PS droplets were introduced into the matrix by using a pin to put a small amount of PS powder on a HDPE disk, and then covering this with another HDPE disk to form a sandwich. The sample was then placed between the top and the bottom disks of the flow cell, both of which were brought into contact with the sample, which was then heated to the testing temperature.

3. Droplet Shape Relaxation Time

We attempted to determine the interfacial tensions by measuring the deformation parameter Def (cf. Eq. 2) of a retracting droplet vs. time, which is known to decay exponentially [Lucinia *et al.* (1997)]:

$$Def = Def_{0} \exp\left(-\frac{t}{\tau}\right) \tag{3}$$

so that the slope of Def vs. t on a semi-log plot can be related the characteristic relaxation time for a single drop, τ. By equating this characteristic relaxation time to that predicted by the Palierne model (Eq.4) [Palierne (1990) and Graebling *et al.* (1993)], the apparent interfacial tension was then calculated from the following relation

$$\tau = \frac{(3 + 2\eta_r)(16 + 19\eta_r)r_o\eta_{m,o}}{40(1 + \eta_r)\Gamma} \tag{4}$$

To obtain images of the relaxing droplet after a large strain, the desired strain was imposed onto a selected drop in the field of view of the microscope which moved the droplet out of the field of view, then the droplet was left to relax at least 40-50 min (which is equal to or greater than the droplet relaxation time) to ensure that the drop had returned to the spherical shape, and then the droplet was moved back into the field of view by imposing the same strain in the reverse direction. A hundred to 200 images were then recorded (10-20 seconds per frame) while the droplet relaxed its shape. For both systems, the droplet size was varied from around a hundred micron up to 400 μm or thereabouts. For system A, with initial drop size of 96 μm shear rate 0.2 1/sec η_r equal to 0.79 and η_r equal to 3150 Pas, the relaxation time of Eq. 3 was 362 sec and the corresponding Γ was 1.66 mN/m. Fig. 3 (a) and (b) shows that the apparent interfacial tension values inferred from Eq. 4 increases with the droplet size. This dependence of apparent interfacial tension on droplet size is likely caused by the contribution of droplet elasticity to the relaxation of the droplet shape. For large enough droplets, relaxation should become slow enough that viscoelastic stresses relax too quickly to influence droplet shape relaxation and hence the rate of relaxation is governed by interfacial tension alone. Thus, the interfacial tension value obtained for large droplets is expected to be the most accurate. Unfortunately, because of the limitation in the ratio of a gap width to an initial droplet size, which was kept at greater than 5, we cannot attain a regime in which the apparent interfacial tension becomes independent of droplet size; see Fig. 3. Therefore, the values of the interfacial tension for the polymer blend systems used in this work were taken from the literature [Brandrup and Immergut (1989)], which are 5.79 mN/m for system A at 147°C, and 5.92 mN/m for system B at 139°C.

From the optical microscope, the droplet images were captured only from the top view, i.e., a view containing the flow and vorticity directions. Since only a projection of the droplet onto the vorticity plane can be imaged from this view, this view cannot determine the true lengths of the principal axes, because two of them

(those in the flow and the shear-gradient directions) are not parallel to the vorticity plane. However, the lengths of these axes can be determined by using the affine angle of rotation of the droplet in the plane containing the flow and shear-gradient directions (Larson 1988) together with the condition of volume preservation, $D_o^3 = abc$ (Almusallam *et al.* 2000).

Although the lengths of the principal axes can be approximated by using the method mentioned above, for convenience we use the lengths of the observable axes, shown in Fig. 4, to describe the behavior of each droplet. Thus, we define a modified deformation parameter Def* as:

$$Def^* \equiv \frac{a^* - c^*}{a^* + c^*} \tag{5}$$

where the asterisk denotes that the deformation parameter is an apparent one obtained from the droplet image projected onto the flow-vorticity plane; see Fig. 4.

4. Transient Deformation

The deformed shapes were observed as a function of time from initial to steady-state shapes. Because the Linkham device has one stationary and one moving plate, a single droplet cannot be viewed continuously from startup of shearing to attainment of steady-state shape, since this droplet will pass out of the viewing plane after imposition of around 10 strain units. However, since the behavior of a given isolated droplet is highly reproducible, the strain dependence of the deformation can be determined by combining the results of several experiments. In experiments of type 1, we first move the droplet out of the viewing window by imposing a shearing strain of less than 40 strain units. After allowing the droplet to relax its shape for at least 40 minutes, an observed shear rate was imposed at the same strain but in opposite direction, eventually bringing the droplet back into the viewing window, where it can be observed during deformation. However, the droplet could not be subjected to a large strain in this type of experiment, since this would move the droplet again out of the viewing window. So, to obtain droplet deformation at large strains, we performed experiments of type 2, in which we sheared continuously, and imaged the droplet each time it passed through the viewing window in its orbit

around the axis of the rotation of the rotating plate. Typically, one orbit would require around 40 strain units. To get a clear image of the droplet without a high-speed camera, we stopped the flow briefly each time the droplet reached the center of the viewing image and video recorded its shape over a period of around 1 second, which is a time much too short for the droplet to relax its shape significantly. Then the flow was resumed again until the droplet again reached the viewing window. By repeating the experiment on droplets of similar size, which were stopped at different times, we could assemble a consistent curve from multiple droplets of the droplet deformation versus time at a given shear rate. In the following, the results from different droplets will be presented using different symbols, showing the consistency of results combined from multiple droplets. In each experiment, the time for one revolution of a droplet was recorded with a stopwatch along with the time shown on the Linksys program. To avoid interactions with the plates, the ratio of the gap width to the initial diameter of a selected drop was kept higher than 10, and only droplets near the center of the gap were observed. The experiment was repeated with more than 10 droplets with initial diameters around 75 ($\pm$10%) μm. were used, and the imposed shear rate was 0.5 s^{-1}. Similar experiments (only type 2) were carried out using other droplet sizes, 52, 110 and 120 μm, but the same shear rate of 0.5 s^{-1}. To separate the effect of shear rate from that of elasticity, another set of experiments were carried out on droplets of different sizes [135, 75; and 46 μm] but in which the shear rate varied inversely with droplet size from 0.28, to 0.5, to 0.8 s^{-1}, In this way we could vary the viscoelastic forces, which increase with increasing shear rate, while holding the capillary number fixed at around 8 by varying the droplet size inversely with the shear rate.

5. Steady-State Deformation and Breakup

From the transient experiments, the required strain to reach steady state can be determined and was found to be around 2500 strain units. To determine the steady-state droplet shape as a function of capillary number, we carried out experiments up to high strains at two different shear rates and for different droplet

sizes. The selected shear rates were 0.3 and 0.5 s^{-1} for system A, and 1 s^{-1} for system B, which are high enough that the needed strain could be achieved within an acceptable time, but not so high that the steady-state droplet shapes are too small to be imaged clearly. In addition to using these two shear rates, different droplet sizes were chosen to vary the capillary number at fixed elasticity. After loading a sample, droplets were allowed to relax to spherical shapes for a period of at least 50 minutes, a bit longer than for the transient experiments described earlier, since some of the droplets used were larger and so needed somewhat longer to relax. A constant shear rate was then applied until a strain exceeding 2500 strain units had accumulated. When a selected droplet passed through the viewing window, the motor was stopped for less than a second and a video movie (speed 25-fps) was then recorded, as described earlier in the description of the experiments measuring transient droplet shapes. To ensure that the steady state deformation had indeed been attained, we repeated imaging the same droplet for several more passes of the droplet through the viewing window over a period of 5 to 10 min. In addition, after turning off the flow the droplet shape relaxation was recorded at a video recording speed of 10-20 seconds per frame for approximately 1 hour.

When the droplet size was varied at fixed shearing rate, we found a critical droplet size above which no steady state-shape was obtained. For these droplets, the unstable shape of the droplet was recorded with time, by imaging the droplet each time it passed through the viewing window (as in the experiments discussed earlier), until the droplet broke.